In-Cylinder Gas Velocity Measurements Comparing Crankcase and Blower Scavenging in a Fired Two-Stroke Cycle Engine

P.C. Miles, R.M. Green and P.O. Witze
Sandia National Laboratories
Livermore, California

ABSTRACT

The in-cylinder flow field of a Schnürle (loop) scavenged two-stroke engine has been examined under conditions simulating both blower and crankcase driven scavenging. Measurements of the radial component of velocity were obtained along the cylinder centerline during fired operation at delivery ratios of 0.4, 0.6, and 0.8. Both mean velocity profiles and root mean square velocity fluctuations near top center show a strong dependence on the scavenging method. Complementary in-cylinder pressure measurements indicate that combustion performance is better under blower driven scavenging for the engine geometry studied.

IN THE PAST TEN YEARS the engine research and development community has demonstrated a renewed interest in two-stroke engine technology. Many manufacturers have new engine designs operating on test stands and in prototype vehicles being road tested. This recent development activity has resulted in the adoption of both crankcase and external blower scavenged designs as the baseline engine configurations. Both design concepts have their advantages and disadvantages, and there seem to be situations where each is best used.

Crankcase scavenging with piston-controlled porting and dry-sump lubrication is certainly the simplest engine configuration from the size/weight/complexity point-of-view. The General Motors CDS2 design and one of the Orbital Engine Company designs are examples of current crankcase scavenged configurations (Wyczalek [1]*). This design offers the potential of improved fuel economy at light load operation due to lower pumping and friction losses. Some disadvantages, however, include the need to either mix or inject lubricating oil into the intake charge and a crankcase design requiring individual cylinder sealing along with the use of roller bearings. In addition, the crankcase pumping by the reciprocating piston leaves little flexibility in controlling the scavenging flow, leading under some conditions to undesirably low scavenging efficiency. The scavenging efficiency can be somewhat improved using crankcase compression with uni-flow scavenging, which requires the use of valves and valve control mechanisms with the associated increase in complexity.

External blower scavenging can be implemented in different configurations. For example, Subaru uses piston-controlled porting and a screw-type compressor; Toyota uses camshaft-driven valves and a roots-type blower; and Orbital employs flywheel mounted centrifugal blowers with piston-controlled porting in two of their current designs (Wyczalek [1]). These blower scavenged engines use wet-sump lubrication systems. The use of an external blower itself adds to the mechanical complexity of the engine, and the additional use of valves further increases the complexity. On the other hand, the use of an external blower and valves can lead to an improvement in the control of the scavenging process and, in turn, an improvement in engine performance. Furthermore, wet-sump lubrication allows the use of common, inexpensive journal bearings and a less-complex crankcase arrangement along with a reduced concern over exhaust catalyst poisoning due to use of improper lubrication oil.

Previous investigations of the scavenging process have been focused on one or the other scavenging mode and not on a comparison of the two. In addition to a global understanding of the good and bad features of the two scavenging methods, a direct comparison of the two could provide engine designers with additional insight as to which method is more suitable for their application. The intent of the work reported in this paper is to characterize and compare the in-cylinder flow fields associated with both crankcase and external blower scavenging configurations, in an engine that can be operated in either mode. In-cylinder pressure measurements are also reported to provide a relative indication of the combustion performance associated with the two scavenging methods. A comparison of this sort provides

* Numbers in brackets designate references at end of paper.

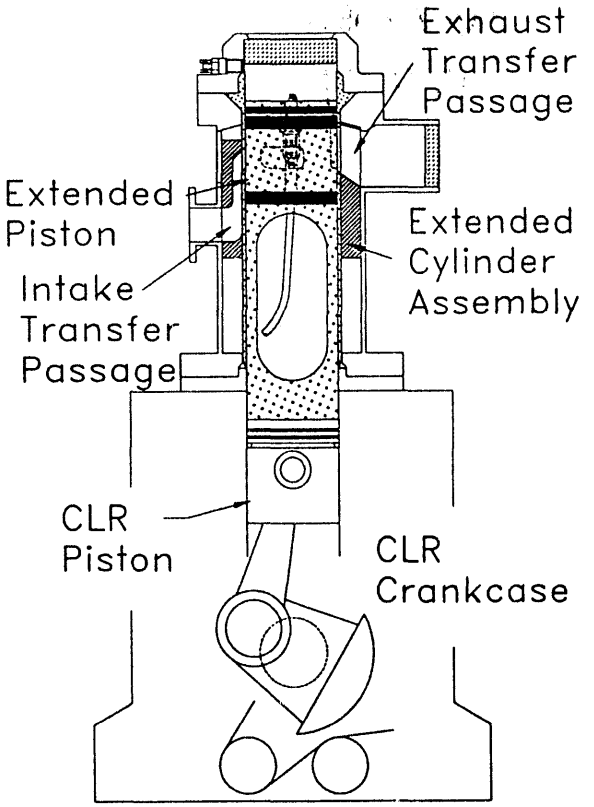

Fig. 1 Two-stroke optical research engine.

information on the general features associated with each flow field, and the possible suitability of each configuration to specific engine geometries.

EXPERIMENTAL DESCRIPTION

OPTICAL RESEARCH ENGINE – The engine used in this study is a modified Cooperative Lubrication Research (CLR) engine, in which the head has been removed and replaced by an extended cylinder assembly (Fig. 1) consisting of an outer structural housing and an inner liner. An extended piston is mounted to the CLR piston and is run unlubricated using a pair of bronze loaded Teflon* rider rings to prevent the piston from directly contacting the liner. The top ring is a sealing ring and is made of Vespel*, a graphite-filled polyimide material. Transfer passages in the annulus between the housing and the liner direct fresh air from the intake manifold to ports in the cylinder wall and channel the exhaust port efflux into the exhaust manifold. The intake transfer passages and the intake ports in the liner have been designed to impart a 'Schnürle-loop' directional characteristic to the flow as it enters the cylinder through the scavenge ports (Groff et al. [2]).

The cylinder head is a simple cylindrical shape and supports a window located above a pancake combustion chamber of the same diameter as the cylinder bore. This configuration allows optical access to better than 80 percent of the cylinder area. Water is circulated through an internal channel in the head flange for thermal control of the window. To reduce the maximum flame-travel distance across the combustion chamber, the spark plug is mounted in the center of the piston crown. This centrally located ignition site improved combustion performance significantly over a sidewall location. An AVL Model QC42D-E piezo-electric pressure transducer is mounted in the head to monitor the in-cylinder pressure, and the crankshaft is instrumented with a shaft encoder with 0.5 crank-angle degree (CAD) resolution. The important geometric characteristics of the engine are listed in Table 1; additional details of the engine configuration are provided by Green and Cousyn [3] and Bopp et al. [4].

SCAVENGING MODES – The mode of scavenging defines the manner by which the in-cylinder flow field is driven during the interval that the intake and exhaust ports are open and gas exchange is taking place. In a crankcase scavenged engine, the pumping action that the piston exerts on the crankcase results in the fresh charge trapped in the crankcase being compressed until the intake ports open. When the intake ports first open, there is a strong flow into the cylinder due to blowdown of the compressed charge in the crankcase. The flow rate into the cylinder subsequently drops rapidly, due to slowing of piston motion as bottom center is approached and the relatively small piston displacement from intake port opening to bottom center. On the other hand, in the case of external blower scavenging a reasonably constant pressure is maintained at the intake ports throughout the gas exchange process. This results in a relatively steady inlet flow through the intake ports without the strong initial in-flow which is characteristic of crankcase scavenging. It should be noted that the above discussion illustrates the principal characteristics of the scavenging flows and has not included the effects of pressure wave dynamics which also influence the scavenging flows.

In our simulations of crankcase and blower scavenging, we use the engine configuration described in

Table 1 Engine Characteristics

Type:	Single cylinder, two stroke w/ piston-controlled porting
Bore:	94.4 mm
Stroke:	95.3 mm
Clearance Height:	9.5 mm
Comp. Ratio (Geom.):	11.0
Comp. Ratio (Eff.):	6.0
Intake Port Opens:	120 CAD
Intake Port Closes:	240 CAD
Exhaust Port Opens:	90 CAD
Exhaust Port Closes:	270 CAD

* Teflon and Vespel are registered trademarks of DuPont.

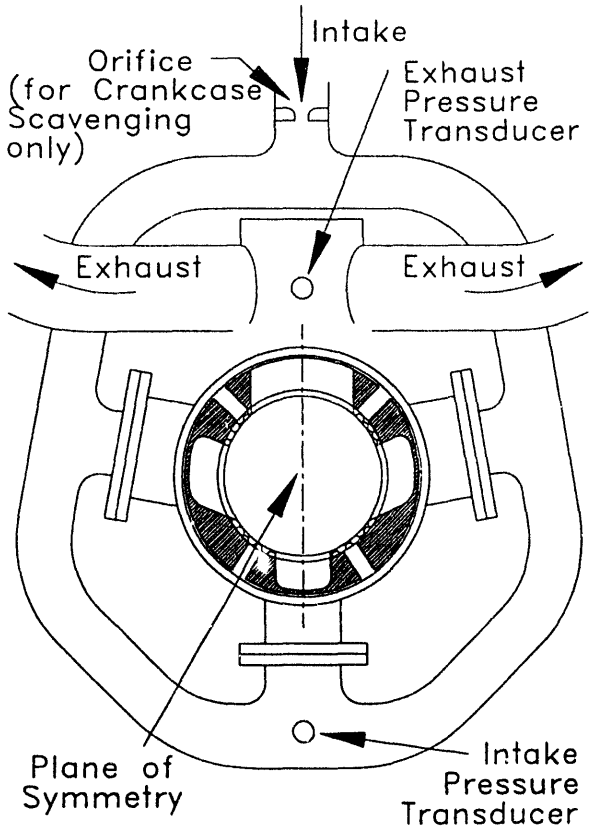

Fig. 2 Plan view of the port layout and manifolding.

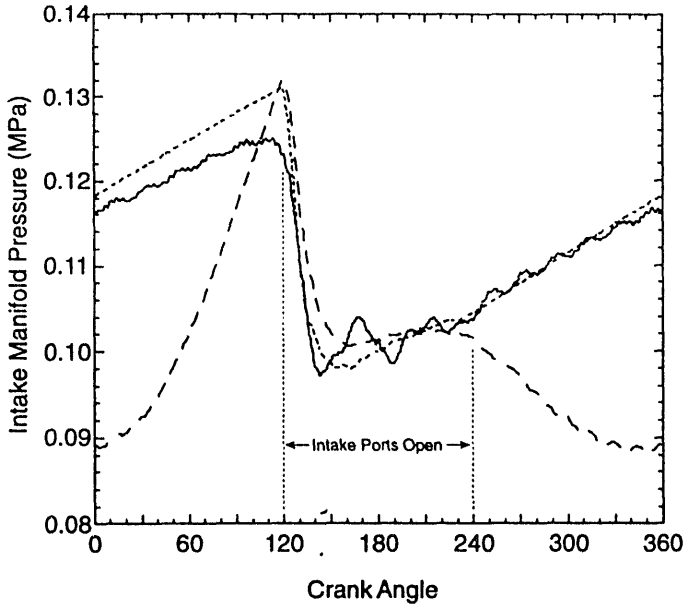

Fig. 3 Computed simulation of the crankcase scavenged intake manifold pressure compared with the measured pressure. —— Measured; – – – Computed, real engine; ------ Computed, simulation of experiment.

the previous section for both scavenging modes. To simulate blower scavenging, fresh mixture is supplied through a critical orifice to large diameter supply lines connected directly to the intake manifold. These supply lines act as a high-volume plenum that maintains a relatively constant pressure in the manifold. Pressure fluctuations due to wave dynamic effects are damped by elbows in the supply lines and a honeycomb section. The pressure at the intake ports (and thus, the mass flow rate) is therefore maintained at a reasonably constant level throughout the time that the intake ports are open. This situation is directly analogous to the case of external blower scavenging. To simulate crankcase scavenging, the orifice metering the flow into the plenum is removed, and a second orifice is inserted between the plenum and the intake manifold (Fig. 2). In this case, the flow into the manifold raises the pressure at the ports while the intake ports are closed. Upon opening of the intake ports, the manifold rapidly blows down into the cylinder, simulating the initial blowdown period of a crankcase scavenged engine. For the remaining portion of the scavenge process, mass flow rates through the intake ports are small due to the restriction of the orifice. The volume of the intake manifold was tailored to obtain an intake port pressure history typical of crankcase scavenging.

Validation of our simulations was performed by Groff [5] using the WAVE intake/exhaust system simulation code developed by Morel, et al. [6]. He compared the measured port pressure histories to computed results for our engine geometry, as well as for an actual crankcase scavenged engine. A comparison of the computed results with experimental measurements at a delivery ratio of 0.52 is illustrated in Fig. 3. Note that a simulation of crankcase scavenging need only simulate the actual intake port pressure from the time the port opens until port closure (120 to 240 CAD.) During the period the ports are closed, the pressure history predicted for the actual engine is simply the pressure within the crankcase, which is of little significance to the scavenging process. While the magnitude of the measured pressure at the time the intake ports open is somewhat less than the prediction (due largely to leakage from the intake ports to the exhaust ports through excessive clearance between the piston and cylinder), the general character of the pressure histories is sufficiently similar to indicate a reasonable simulation of crankcase scavenging.

ENGINE OPERATION – The nature of two-stroke engine scavenging is such that the processes involved depend strongly on manifold and cylinder conditions resulting from the previous engine cycle. Thus only continuously fired operation should be used in order to create a true representation of the actual phenomena. This precludes using a skip-firing ignition strategy to reduce the thermal loading of the windows. In order to achieve realistic scavenging conditions without risking window failure, we adopted a "burst-fired" ignition strategy, wherein the engine was fired on 13 consecutive cycles followed by 27 consecutive cycles of motored operation. Fig. 4 illustrates a typical pressure history of the fired cycles for crankcase scavenging at a delivery ratio of 0.60. Although absolute magnitude of the measured pressures varies, as does the cyclic variability, these data are representative of the nature of the data

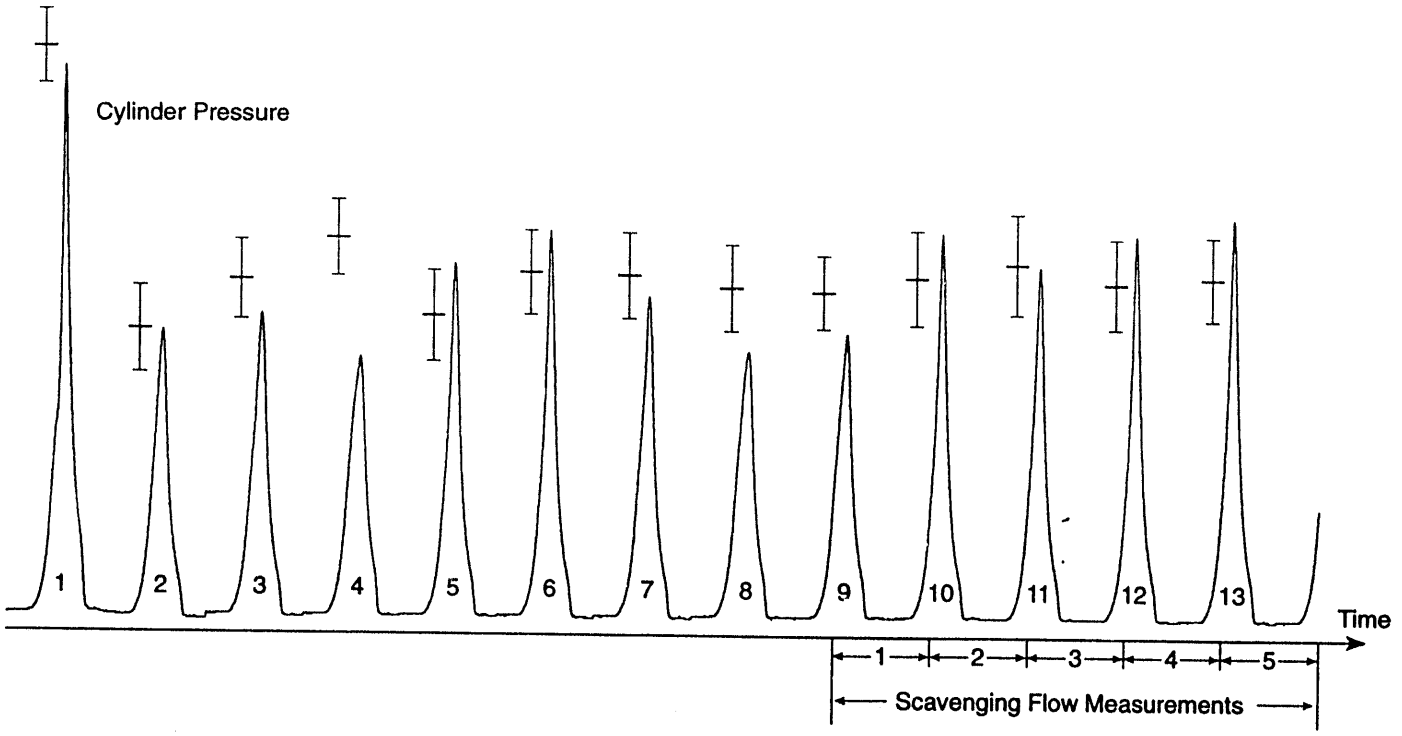

Fig. 4 Typical pressure histories for the 13 consecutive fired engine cycles.

obtained for either crankcase or external blower scavenging over the delivery ratio range investigated. The first fired cycle exhibited the highest pressure; thi is the only cycle that was perfectly scavenged, being preceded by 27 motored cycles. The second through ninth cycles exhibited a complex transient behavior, which varied with both delivery ratio and scavenging mode. A preliminary statistical analysis, based on 40 such fired bursts, demonstrated that the mean and rms (root mean square) fluctuation of the measured peak pressure and the crank-angle at which peak pressure occurs had converged to reasonably constant levels by the tenth cycle. The results of this analysis for the mean and rms fluctuation associated with each cycle of Fig. 4 are indicated by the heavy horizontal lines and error bars, respectively. Cycles 10 through 13 were therefore considered to be representative of steady-state operation. Combustion performance was determined from the in-cylinder pressure histories of these four cycles. For measurements of the scavenging flow field five cycles were used — from the ignition crank-angle of the ninth cycle to the same angle of the motored cycle immediately following the fired burst. The engine operating conditions used in this study are summarized in Table 2.

Table 2 Operating Characteristics

Engine speed:	800 RPM
Fuel (premixed):	Propane
Equivalence Ratio:	1.0
Delivery ratio:	0.3 - 0.85 (variable)
Firing strategy:	Burst fired operation
Firing sequence:	13 cycles fired
	27 cycles motored
Ignition timing (1st fired cycle):	7.5 BTC
Ignition timing (other cycles):	22.5 BTC

LASER DOPPLER VELOCIMETRY

PREVIOUS STUDIES OF SCAVENGING FLOWS – Laser Doppler velocimetry (LDV) has been used to examine in-cylinder flow fields in IC engines for more than fifteen years. However, only within the last ten years has this technique been applied to two-stroke engines with the majority of the significant work occurring in the last five years. Much of the work appearing in the literature involves studies of the flows at the ports or in the transfer passages (e.g., Ikeda [7]). Only a few previous investigations involved measurements within the cylinder or combustion chamber. For example, Obokata et al. [8] have studied the flow in the combustion chamber of crankcase-scavenged engines under both motored and fired conditions. Their results illustrate an apparent dependence of the mean flow in the combustion chamber during scavenging on whether or not the engine was fired. On the other hand, they found that this dependence weakened significantly near the time of ignition, with the turbulence being spatially uniform and also independent of whether or not the engine was fired. In 1992 Fansler and French [9]

published the results of a comprehensive study in which they mapped the in-cylinder and transfer port flow field characteristics of a crankcase scavenged, two-stroke engine operating under motored conditions. Their results revealed the presence of the classic scavenging loop characteristic of Schnürle scavenged designs, and illustrated a high degree of flow-field complexity. Substantial large scale cyclic variations were inferred, as was the evolution and breakdown into turbulence of the scavenging-loop vortex.

LDV SYSTEM AND DATA REDUCTION – Laser Doppler velocimetry measurements of the in-cylinder radial velocity were obtained with a custom fiber-optic LDV probe which was designed and fabricated in-house. The modular design of the probe head permits laser light emerging from the optical fibers to be collimated into beams of various diameters, thus providing the equivalent of beam expansion capability. Complementary collection optics maintain the desired relationship between the probe volume size and its image on the core of the collection fiber. In the configuration used in this work, the collimated beams are approximately 3.9 mm in diameter at the $1/e^2$ intensity contour. A 310 mm focal length transmitting lens focuses the beams to measured waist diameters of 52 μm at the LDV probe volume. Such tightly focused waists are required in order to obtain sufficient signal levels with the backscatter collection geometry employed. The beam spacing in the probe head is 50.0 mm, giving a fringe spacing of 3.21 μm with the green line (514.5 nm) of an Argon ion laser. Titanium dioxide seed particles are generated from the high-temperature thermal decomposition of titanium tetra-isopropoxide, using an apparatus similar to that described by Okuyama et al. [10]. A differential frequency shift of 10 MHz was used, and the Doppler signals were band-pass filtered between 2 and 50 MHz for a measurement bandwidth of -25 to 130 m/s. The filtered signals are processed with a counter type processor (TSI 1990C), which was operating in a single-measurement-per-burst mode and set to count the time for 8 fringes with a 1% validation criterion. Velocity data were subsequently transferred, along with simultaneous crank-angle readings, to a laboratory computer.

Measurements of the radial component of velocity were obtained along the cylinder centerline at 12 axial locations spaced 8.0 mm apart. The uppermost measurement location was 4.0 mm below the lower surface of the head, and the lowest location was approximately 13 mm above the piston crown at bottom center. The axial coordinate z, identifying these locations, has its origin at the lower surface of the head. The measured radial component of velocity lies in the plane of symmetry defined by the cylinder port geometry. This plane is shown by the dashed line in Fig. 2. Velocities in this plane are identified as positive when the flow is towards the exhaust port. Measurements were obtained under firing conditions over 20 fired bursts; only those data obtained within the 5 representative scavenging cycles shown in Fig. 4 were retained for further analysis. The velocity/crank-angle pairs obtained during these 100 representative cycles are sorted by crank-angle into bins 2 CAD wide for computation of the velocity statistics. Results are reported only for those data obtained when the distance from the probe volume to the ground electrode of the spark plug exceeded 3.6 mm or, equivalently, 7.0 mm from the piston crown. Due to noise associated with light scattered from these surfaces, the data obtained closer to the piston are not considered to be reliable.

Average data rates were quite high, and each bin typically contains over 500 velocity measurements. During portions of the expansion stroke, however, the velocity statistics reported may be based on fewer than 100 velocity measurements. Both prior to exhaust port opening, and particularly between about 100 and 120 CAD (just before the intake ports open), data rates can be quite low. Although the in-cylinder velocity field during these periods is not of primary interest in this study, the low data rates observed raise questions about the possibility of a seed density bias which may affect the statistics later in the scavenging process. If the TiO_2 seed particles undergo an adverse change in their light scattering properties during combustion [11], such that packets of burned residual gases are characterized by significantly lower data rates than packets of fresh charge, then the velocity statistics obtained during periods in which both fluids are present in an essentially unmixed state will be biased toward the velocities characteristic of the fresh charge. Quantitative evaluation of the magnitude of this bias is not straightforward, since LDV data rates may be affected by both number density of suitable seed particles as well as gas velocity. By comparing data rates during periods of similar gas pressure and velocity, however, it is possible to estimate the significance of this effect. For this purpose, LDV data rates observed in the period of peak radial velocity during cylinder blowdown (~98 CAD) have been compared with data rates observed later in the scavenging process when equal radial velocities are encountered. The in-cylinder pressure during this period of blowdown is about 0.14 MPa, or 40% higher than the pressure characteristic of the scavenging process. Typically, data rates later in the scavenging process are about 30% higher than those observed during cylinder blowdown. Accounting for the pressure difference, we estimate that data rates characteristic of fresh charge are roughly 80% higher than those characteristic of residual gases. Some potential for bias of the velocity statistics therefore exists, but this potential will be rapidly reduced by mixing. We believe that any statistical bias which may exist is of secondary importance. Further, we conclude from the above discussion that the low data rates encountered in some portions of the expansion stroke are due primarily to low gas velocities. It is noteworthy that because rms velocity fluctuations are low during these periods, fewer samples are required for convergence of the mean velocities.

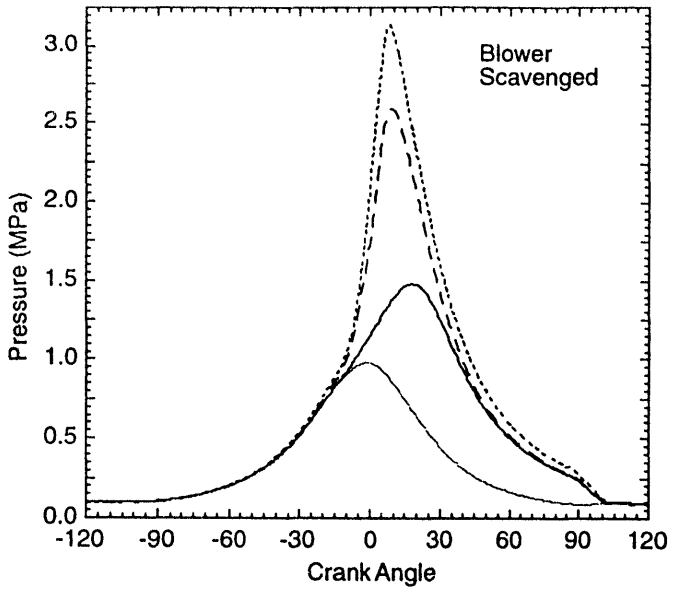

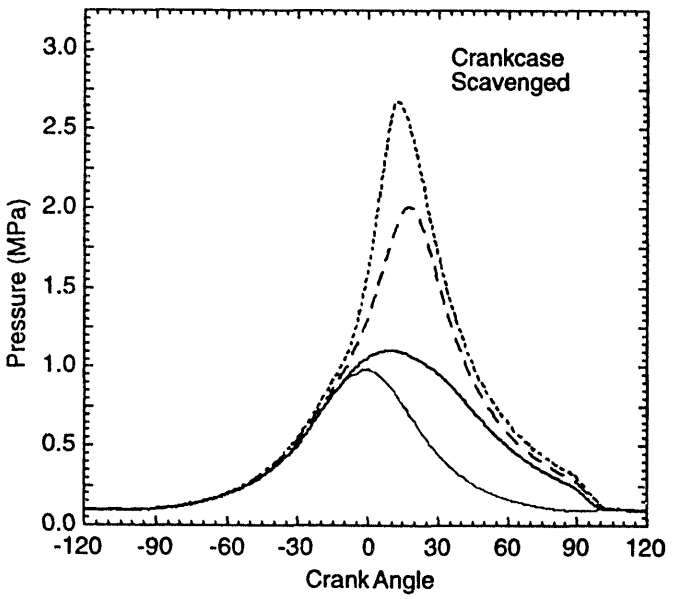

Fig. 5 Typical in-cylinder pressure records for different delivery ratios, compared with the motored pressure for DR=0.40. —— DR=0.40; – – DR=0.60; ····· DR=0.80; —— Motored, DR=0.40.

PRESSURE MEASUREMENTS

The single-cycle pressure records presented in Fig. 5 were selected to be representative of the average cycle for each condition. Because the motored pressure is weakly dependent on the delivery ratio (DR), it is shown for DR=0.40 for a better comparison with the fired pressure data for the slowest burning case. The results shown reflect the better combustion performance for blower scavenged (BLS) operation and higher delivery ratios. For crankcase scavenged (CCS) operation at DR=0.40, peak pressure actually occurs earlier than for the higher delivery ratios because combustion is so slow that cylinder volume expansion due to piston motion dominates the pressure record.

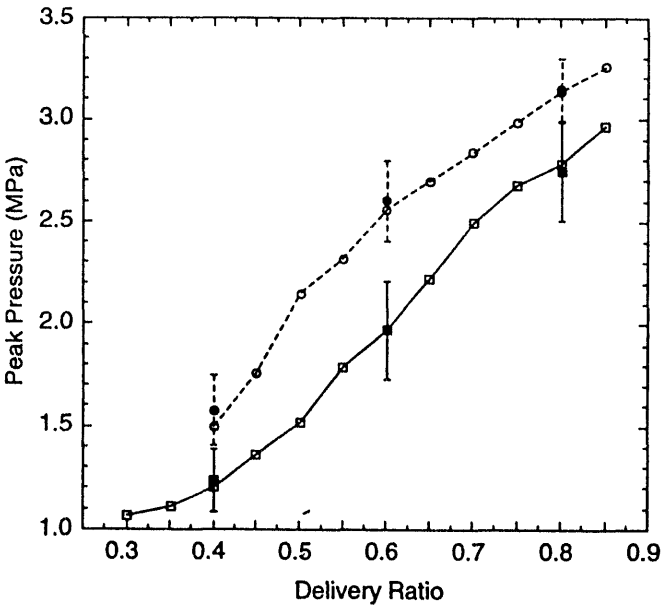

Fig. 6 Comparison between BLS and CCS mean peak pressure as a function of delivery ratio. The open symbols indicate measurements for an average of 160 cycles, while the solid symbols represent an average of approximately 960 cycles; the bars indicate the range of one standard deviation.--●-- Blower scavenging; —□— Crankcase scavenging.

Ensemble-averaged measurements of peak pressure are presented in Fig. 6 as a function of delivery ratio. Misfires which occur during the 9 'transient' cycles of the burst-fired sequence limit the delivery ratios at which steady operation is achieved to those greater than 0.4 for BLS operation and greater than 0.3 for CCS operation. Because the misfires occur during the transient portion of the sequence, our ability to achieve steady operation for CCS at lower delivery ratios does not necessarily imply that CCS extends the lower delivery ratio limit for steady operation. It would appear, however, that at the lower delivery ratios the CCS process is less perturbed by the factors causing the transient behavior depicted in Fig. 4. If a misfire occurs in any cycle of the fired burst, the entire burst is excluded from the computation of the pressure statistics. Peak pressures achieved under BLS conditions are consistently higher than those achieved under CCS conditions. Furthermore, BLS rms fluctuations in peak pressure are less than the CCS fluctuations at all but the lowest delivery ratio. These trends are indicative of better overall combustion performance. This difference in performance could be due to better scavenging efficiency, stratification of fresh mixture and residuals, or turbulence levels during the combustion process.

Results for the crank-angle of peak pressure are given in Fig. 7. BLS has a nearly linear advance in the time of peak pressure with increased delivery ratio, whereas CCS shows this behavior only for DR≥0.55. In this region, CCS burns slower than BLS, which is consistent with the peak pressures presented earlier in

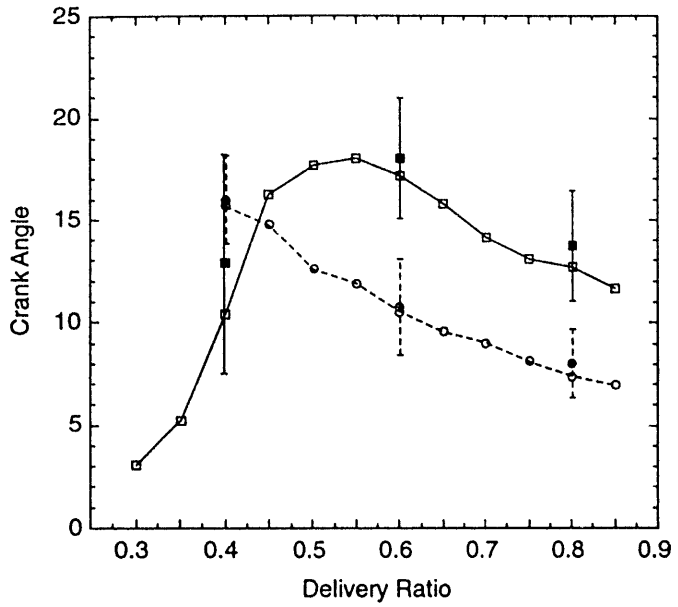

Fig. 7 Comparison between BLS and CCS mean crank angle of peak pressure as a function of delivery ratio. ---o--- Blower Scavenging; —□— Crankcase Scavenging.

Fig. 6. Below DR=0.55, the time at which CCS reaches peak pressure rapidly approaches top dead center (TDC) as the delivery ratio is lowered. As noted above, this behavior is a result of combustion being so slow that piston motion dominates the location of peak pressure. The fact that this trend is totally absent with BLS is again indicative of better combustion performance. Note that the rms fluctuations in the crank-angle of peak pressure are significantly less at all delivery ratios for BLS operation.

Normalized unit-area histograms (probability density functions) of peak pressure and its crank-angle location are given in Fig. 8. For the six different conditions shown, 960 engine cycles, less the misfire cycles mentioned earlier, were analyzed. Except for the CCS case for DR=0.40, the shape of the histograms is generally as expected. Peak pressure tends to be skewed to the low side, and a corresponding skewness to the high side is seen in the crank-angle of peak pressure. This is indicative of cyclic variability characterized by occasional poor combustion performance relative to the mean.

The case of CCS for DR=0.40 is distinctive in that the peak pressure histogram is highly skewed, and the crank-angle of peak pressure is bi-modal. This behavior is the result of two very different combustion modes. The mode characterized by later crank-angles of peak pressure is actually the better performing one. For the engine cycles in this group, heat release was significantly greater than volume expansion from piston motion, such that a distinct maximum occurred in the pressure well after TDC. For the other mode, the heat release was so slow that the pressure history is only slightly increased from the motored pressures. This also explains the skewed distribution of the peak pressure, since the motored peak pressure for this case is 0.99 MPa. Thus, the peak pressure histogram cannot extend below this value, and because no misfires occurred, the minimum value of peak pressure must be somewhat greater. Similarly, rms fluctuations in peak pressure are forced to be artificially low, which explains the higher rms pressure fluctuations observed for BLS at this delivery ratio, despite other indicators of better combustion performance.

MEAN VELOCITY STATISTICS

In this section we present ensemble-averaged mean velocity measurements for the radial component in the plane of symmetry identified in Fig. 2. Comprehensive results for DR=0.60 are presented first, with emphasis on a direct comparison between blower and crankcase scavenging. Following this, selected results comparing delivery ratios of 0.40, 0.60, and 0.80 are presented.

BLOWER VS. CRANKCASE SCAVENGING – In Fig. 9 the mean velocity histories of all data recorded for DR=0.60 are summarized. The length of the crank-angle records varies because the piston obstructs some measurement locations during part of the cycle. At the beginning of the time records, prior to exhaust port opening (EPO) the flow field in the cylinder is quiescent for CCS, and a nearly constant and spatially uniform negative velocity exists for BLS. Blowdown is indicated by a highly transient, short duration flow in the radial direction toward the port. Note that the blowdown flow begins before EPO (defined as when the piston crown clears the port), at the instant the top piston ring clears the port. As might be expected, the velocity of the flow decreases with increased distance from the port, and the velocities are virtually identical for the two scavenging schemes.

At all locations, blowdown is followed by a reverse flow indicative of backflow from the exhaust manifold. Oscillations, which may due to pressure waves in the exhaust manifold, are superimposed on this reverse flow (see Appendix). Next, there is a strong surge of fluid motion due to the incoming fresh charge when the intake ports open (IPO). Compared to BLS, the intake flow velocities are considerably greater for CCS, and motion of the gas begins earlier at each measurement location. After reaching a maximum, the CCS velocity decays quickly and undergoes a flow reversal at all but the upper three measurement locations. This reversal begins shortly after bottom dead center (BDC), and may be caused by volume reduction due to piston motion. The flow then reverses again at, or just prior to, intake port closure (IPC), indicative of resumed flow toward, and most likely out, the exhaust port. Finally, when the exhaust port closes (EPC) the flow again goes negative near the piston crown.

In contrast, because the intake mass flow rate is more constant for BLS, positive velocities created by the intake flow persist at all locations up to IPC. However, it also takes much longer for a positive velocity to become established at the locations closest to the ports. It will be

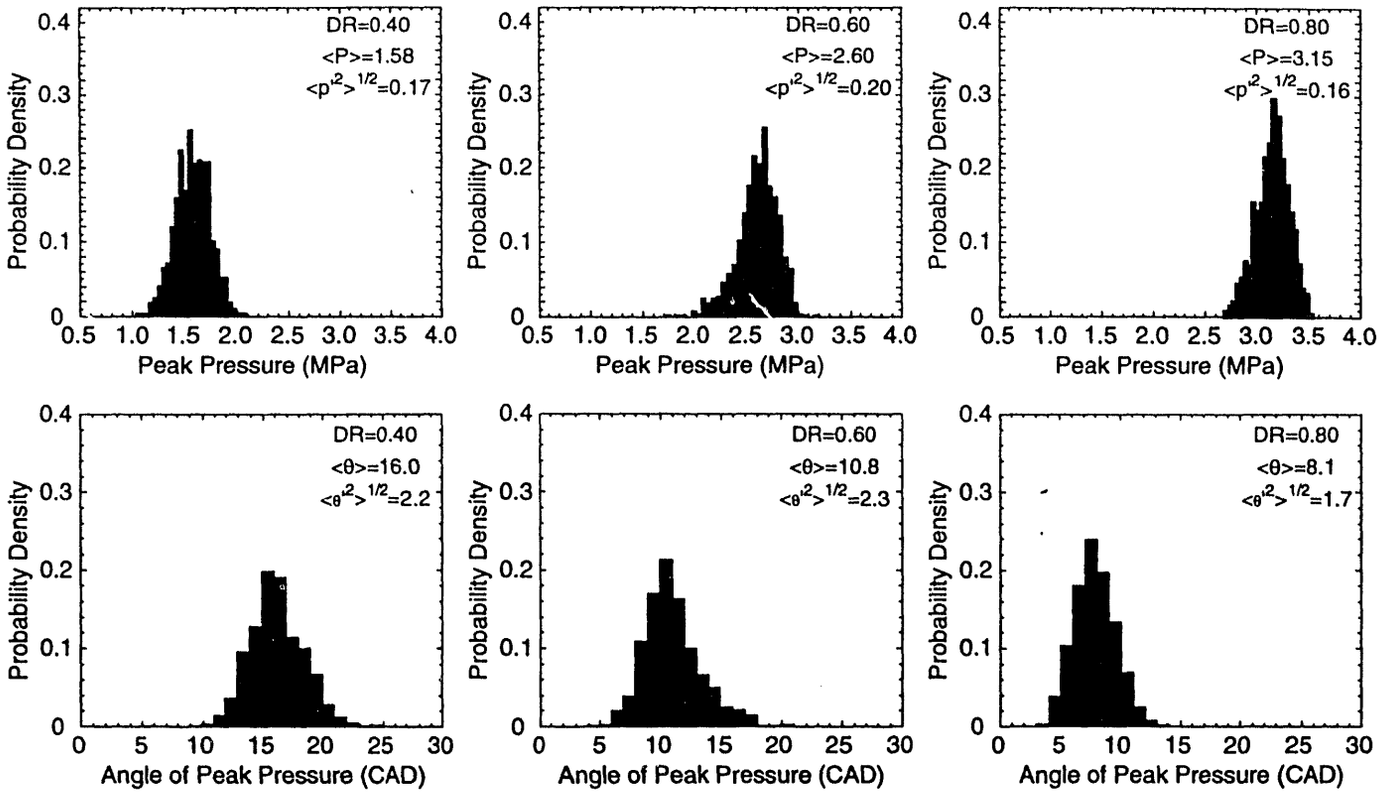

a) Blower scavenged in-cylinder pressure statistics.

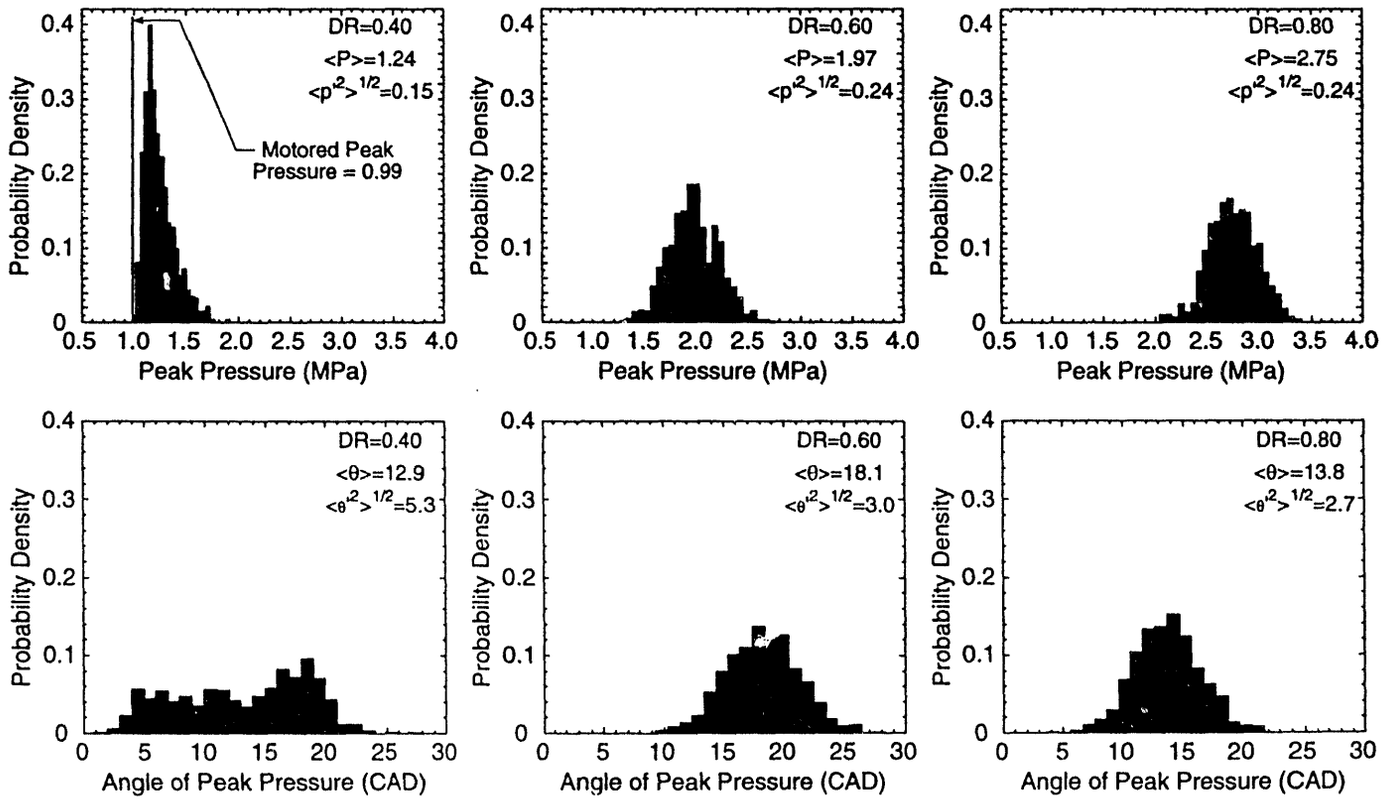

b) Crankcase scavenged in-cylinder pressure statistics.

Fig. 8 Histograms of peak pressure and crank-angle of peak pressure. a.) Blower scavenged b.) Crankcase scavenged

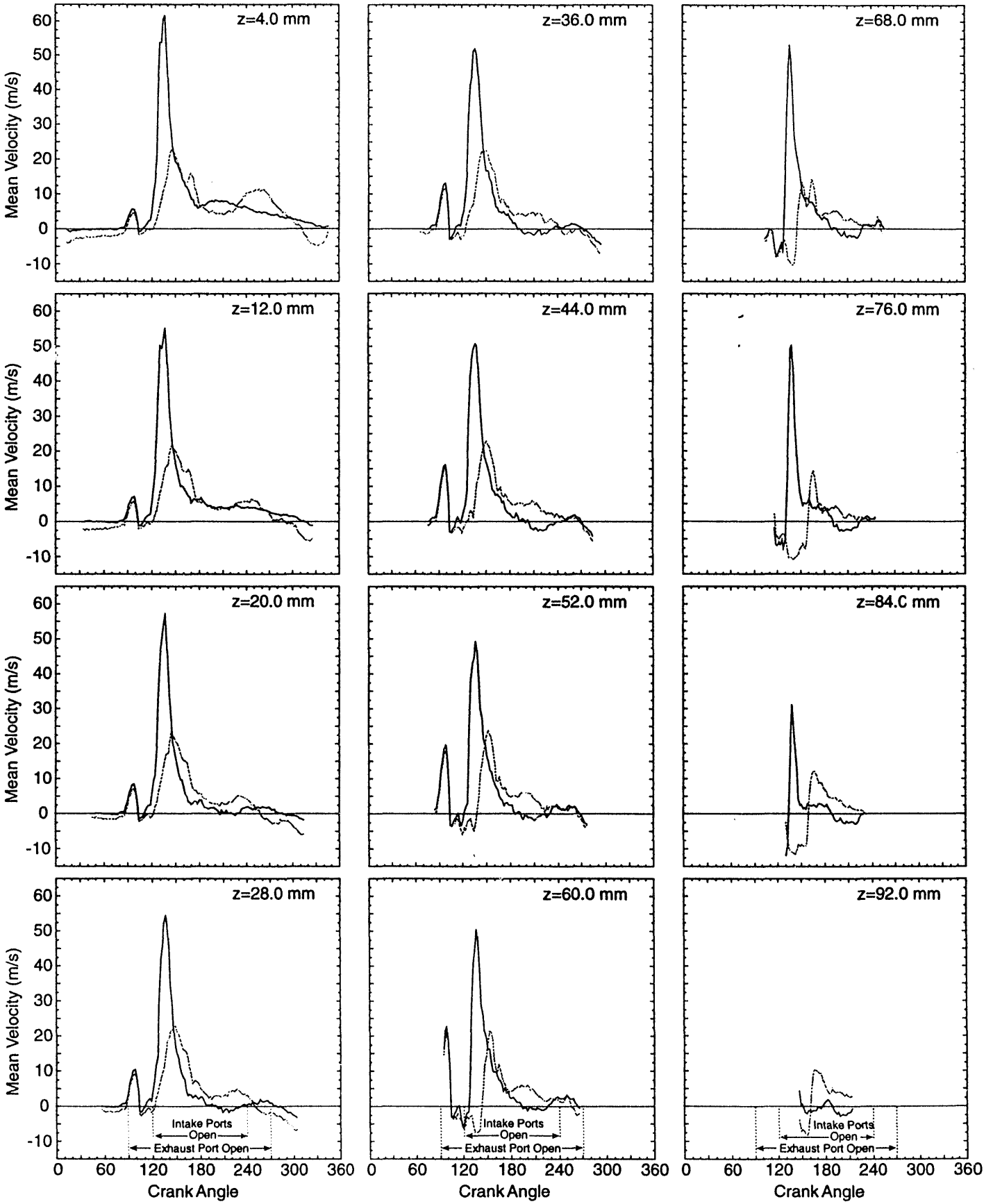

Fig. 9 Comparison of BLS and CCS mean velocity histories for DR=0.60. —— Crankcase Scavenging; ------ Blower Scavenging.

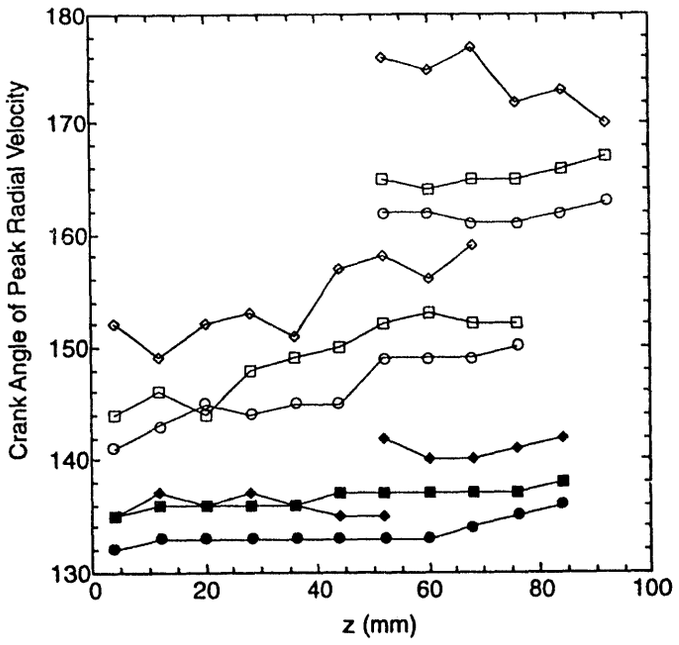

Fig. 10 Crank-angle of maximum gas velocity during intake. Open symbols represent blower scavenged data and filled symbols represent crankcase scavenged data. —◆— DR=0.40; —□— DR=0.60; —○— DR=0.80.

shown shortly that this is because a large, tumbling vortex structure forms in the early stages of induction of the fresh charge. Later on, as the intake ports open more fully, the flow experiences a rapid transition. Prior to this transition, the flow near the bottom of the cylinder (z=76–92 mm) is negative; after this transition, the flow is characterized by a uniformly positive centerline velocity. The double peak in velocity at z=68 mm indicates the time at which the transition between these two flow patterns occurs. This behavior can be seen more clearly in Fig. 10, where we have plotted the crank-angle of the velocity maxima as a function of axial position. In the region of z=52–72 mm, where double peaks in velocity occur for all three delivery ratios, we show both values. The transition in flow pattern is so abrupt that we suspect it may be due to instability of the intake jets with regard to attachment to the piston top or the cylinder walls. It is also interesting that a second peak in velocity within the upper portion of the cylinder occurs at the same time as the transition to a uniformly positive flow. This implies that the transition results in a velocity acceleration at the top of the cylinder as well. As will be seen below, the centerline velocity profile after the transition occurs is characterized by two local maxima. Compared with the results also shown for CCS, it is evident that no similar transition occurs at the higher delivery ratios, although evidence of a similar, earlier transition may be seen for CCS at DR=0.40.

The nature of the flow field is more clearly seen in the vector plot diagrams to be shown next. They will be presented in groups corresponding to periods of the engine cycle, beginning with the blowdown phase shown in Fig. 11. Prior to blowdown, the flow field is reasonably quiescent for both scavenging schemes. The blowdown process actually begins when the top piston ring clears the top of the exhaust port, such that when the piston crown clears the port at 90 CAD, flow out the port has already commenced. As might be expected, the velocities are largest near the piston, but a positive radial flow exists along the entire length of the cylinder axis. The flow reversal immediately following blowdown that was mentioned previously is seen to also penetrate to the top of the combustion chamber. This flow reversal persists until IPO, and may be considered to represent an initial condition for the scavenging flow field.

In Fig. 12 we present vector diagrams for the early scavenging period from IPO at 120 CAD to 140 CAD. At 120 CAD, the distinct reverse flow which has persisted from the blowdown period is still seen near the piston for both scavenging schemes. Low in the cylinder, the existing reverse flow may be enhanced by an induced, entrainment-like flow created by the starting jet exiting the boost port. At this instant there is also the beginning of a positive flow near the top of the cylinder for CCS that is indicative of a further response to the initial intake flow. Because the starting jet for BLS is much weaker, it takes longer to penetrate to the top of the cylinder.

By 125 CAD, both scavenging schemes show a dominant tumble vortex structure, but with far greater velocities near the top of the cylinder for CCS. From this point on, the two flow fields develop in very different ways. For BLS, the vortex structure continues to build strength, whereas for CCS the vortex structure does not appear to persist very long, and by 135 CAD a uniformly positive flow is established along the cylinder centerline. Note that this positive velocity profile does not necessarily imply that tumble vortex motion has ceased, only that the flow profile is no longer dominated by a single large tumble vortex. More likely, a transition in the direction of the intake jets has pushed the fluid characterized by negative radial velocities off the cylinder centerline, and large vortical structures (with a significant tumble component) persist in the flow field. Due to the rapid fall-off of the mass flow rate through the intake ports for CCS, however, this flow has begun to decay by 140 CAD. Finally, it is clear that both scavenging flows have penetrated well to the top of the combustion chamber.

Vector plots for the middle part of the scavenging period, bottom center ±30 CAD, are shown in Fig. 13. The BLS velocity profile, initially dominated by a tumble vortex, undergoes the above noted transition to a uniformly positive centerline flow during this period. The radial velocity profile initially changes quite slowly, and differs little at 158 CAD from the profile shown at 150 CAD. By 161 CAD, however, radial velocities are uniformly positive*, and quickly evolve to the double maxima structure shown at 165 CAD. As the crank-angle increases, the lower maximum moves toward the bottom

* As noted in the discussion of the early CCS flow, the positive velocity profile does not necessarily imply the cessation of vortical motion with a 'tumble' component.

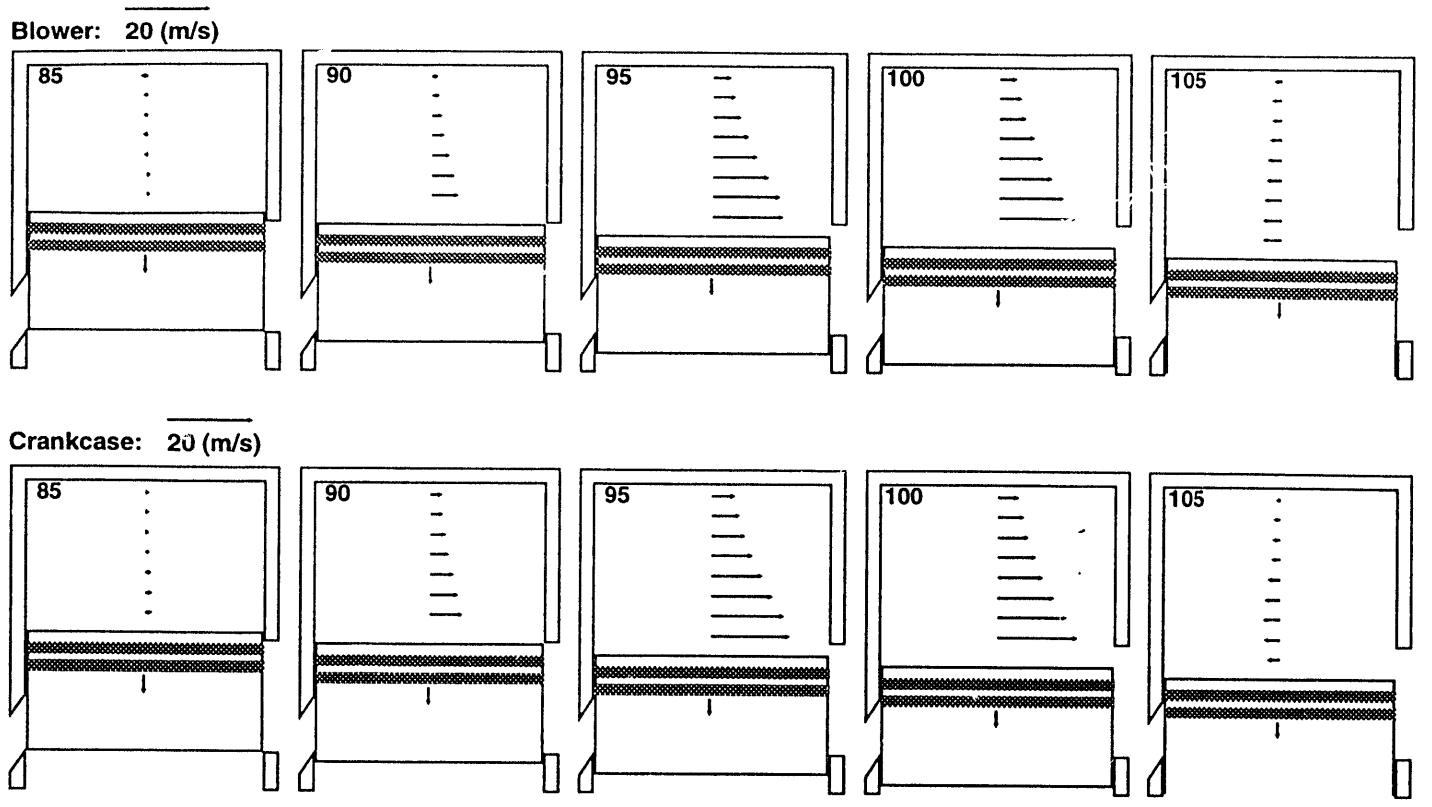

Fig. 11 Comparison of blower and crankcase scavenged velocity profiles during blowdown for DR=0.60. The crank-angle for each profile is given in the upper left corner of each figure.

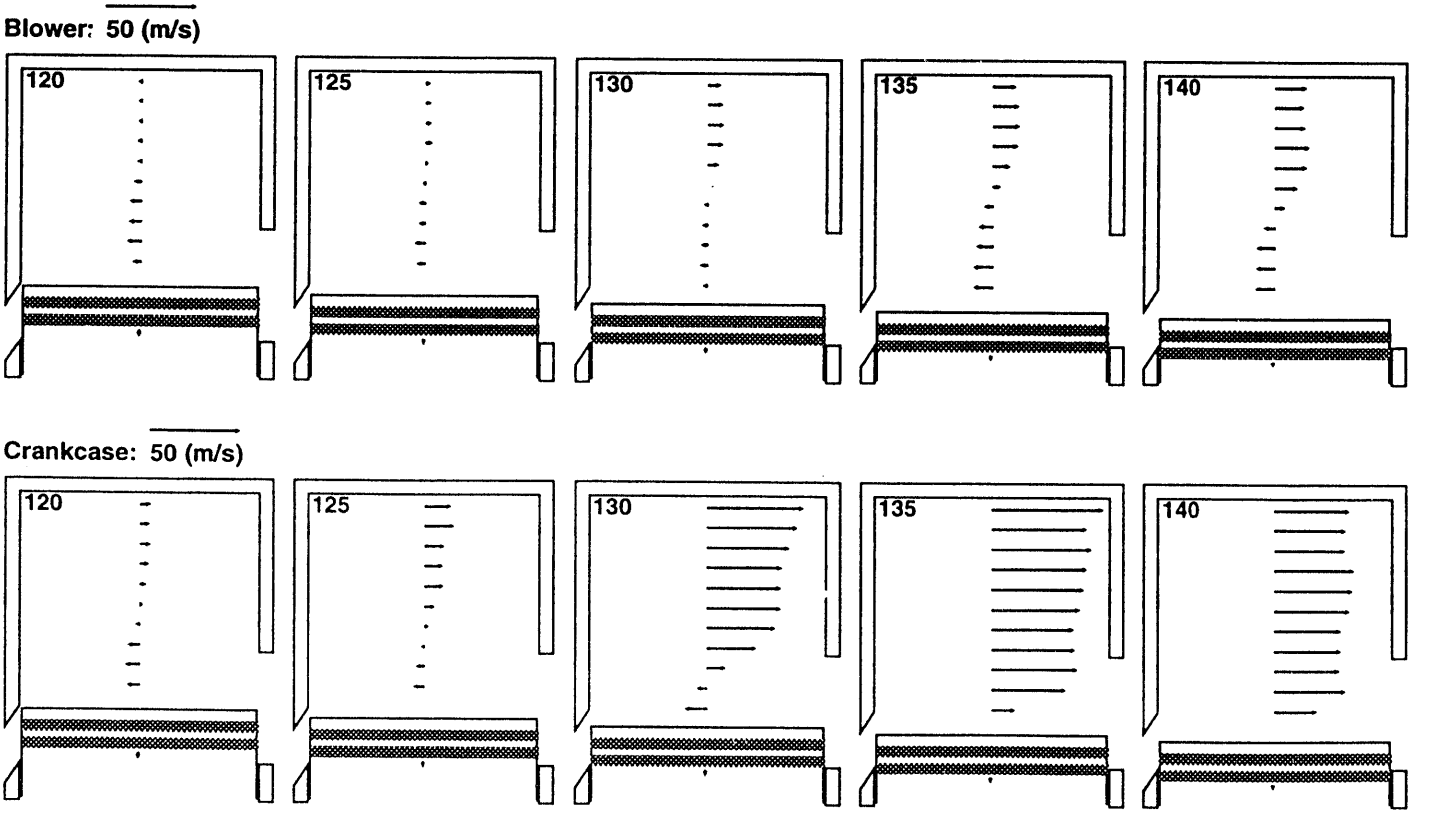

Fig. 12 Comparison of blower and crankcase scavenged velocity profiles during the early scavenging period for DR=0.60. The crank-angle for each profile is given in the upper left corner of each figure.

Fig. 13 Comparison of blower and crankcase scavenged velocity profiles during the mid-scavenging period for DR=0.60. The crank-angle for each profile is given in the upper left corner of each figure.

of the cylinder, persisting beyond 180 CAD. The centerline velocities remain positive thereafter, although with decreasing strength and with considerably lower magnitude than those characterizing the early CCS profile.

In contrast, the radial velocities low in the cylinder are initially decreasing rapidly for the CCS flow during this period. By 150 CAD a structure reminiscent of the BLS profile, characterized by two velocity maxima, has developed. The upper maximum, at the top of the cylinder, remains well defined throughout this period, while the lower, broader maximum loses definition and disappears by 190 CAD. At 195 CAD and beyond, the lower portion of the CCS profile has become quite complex, and is characterized by radial velocities of lesser magnitude than seen in the BLS flow. The smaller velocities characterizing the CCS profile are to be expected due to the larger delivery rates for BLS during this part of the cycle. Towards the end of this period, the CCS flow again appears to contain a dominant tumble vortex.

Results for the final stages of the scavenging process, from just before IPC to EPC, are shown in Fig. 14. Once again, the flow fields for the two cases are quite different; while one appears somewhat orderly, the other seems quite complex. Two features are common to both flows, however. First, near the top of the combustion chamber, relatively large positive velocities exist. For BLS these velocities can be over twice the magnitude of those observed in the CCS flow. This feature can be simply explained as being due to the larger fresh charge delivery rate during this portion of the cycle for BLS conditions. As the open area of the intake port is reduced by piston blockage, renewed jets of high velocity fluid are directed toward the top of the combustion chamber, giving rise to the higher velocities. Second, just after IPC, there is a persistent positive flow near the top of the piston, indicative of a piston driven flow out the exhaust port.

In Fig. 15 we present velocity profiles for the compression stroke after EPC. Both flows during this period appear to be characterized by the compression of a dominant tumble vortex, but the difference in velocities from the top of the combustion chamber to the top of the piston, and thus the mean shear stresses, are everywhere greater for BLS. This more energetic tumble motion is likely due to the renewed jet of fresh charge observed in the latter part of the BLS flow. We will show in a figure to be presented later that the rms velocities near TDC for BLS are greater than for CCS, a direct result of the different flow fields shown here.

EFFECT OF DELIVERY RATIO – Figure 16 illustrates the effect of delivery ratio on velocity at two locations. The most striking aspect of this figure is the high degree of self-similarity in the velocity histories as the delivery ratio is varied. Although the phasing of the dominant features can be seen to depend on delivery ratio, the form of the velocity histories changes little. This observation is generally true at all axial locations, and it is clear that the major distinguishing (and differentiating)

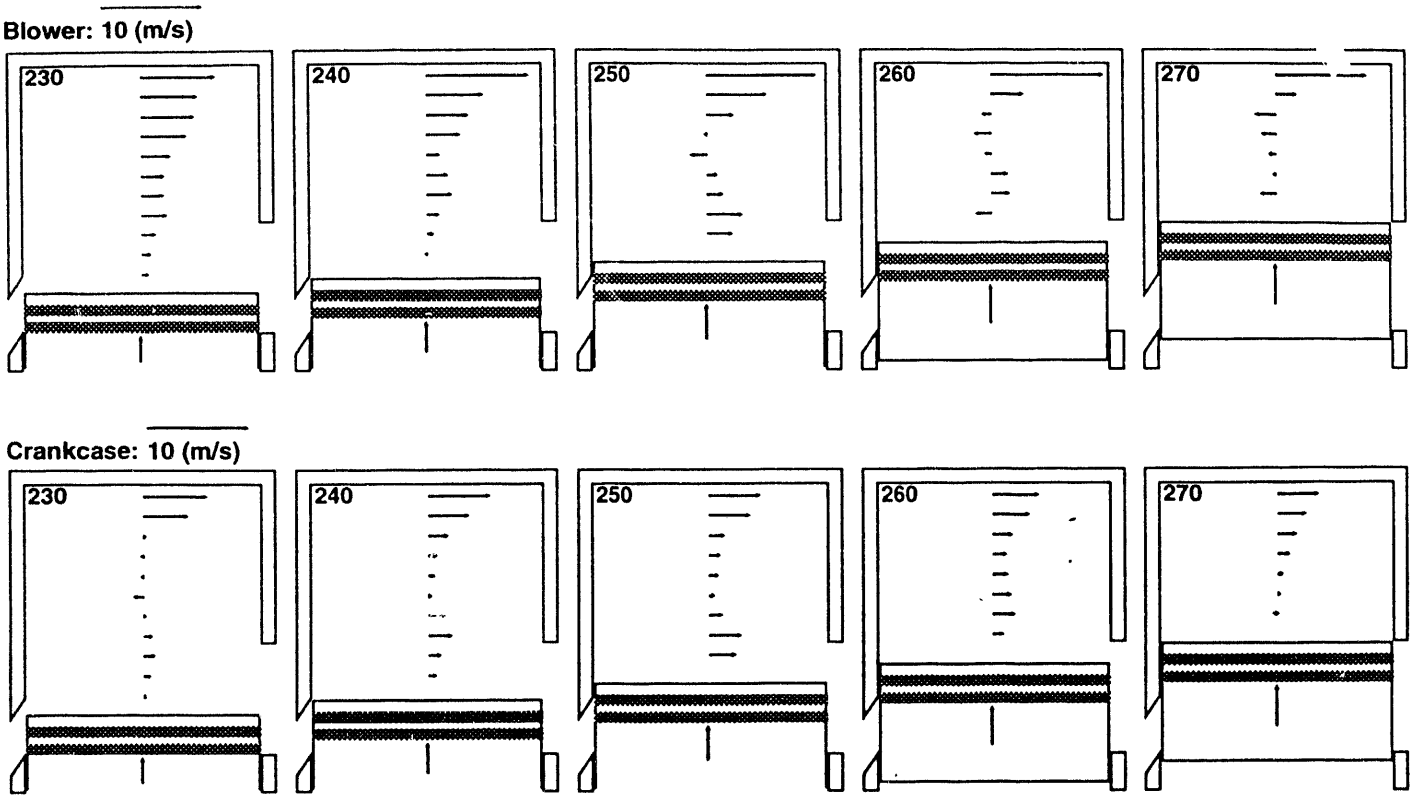

Fig. 14 Comparison of blower and crankcase scavenged velocity profiles during the late scavenging period for DR=0.60. The crank-angle for each profile is given in the upper left corner of each figure.

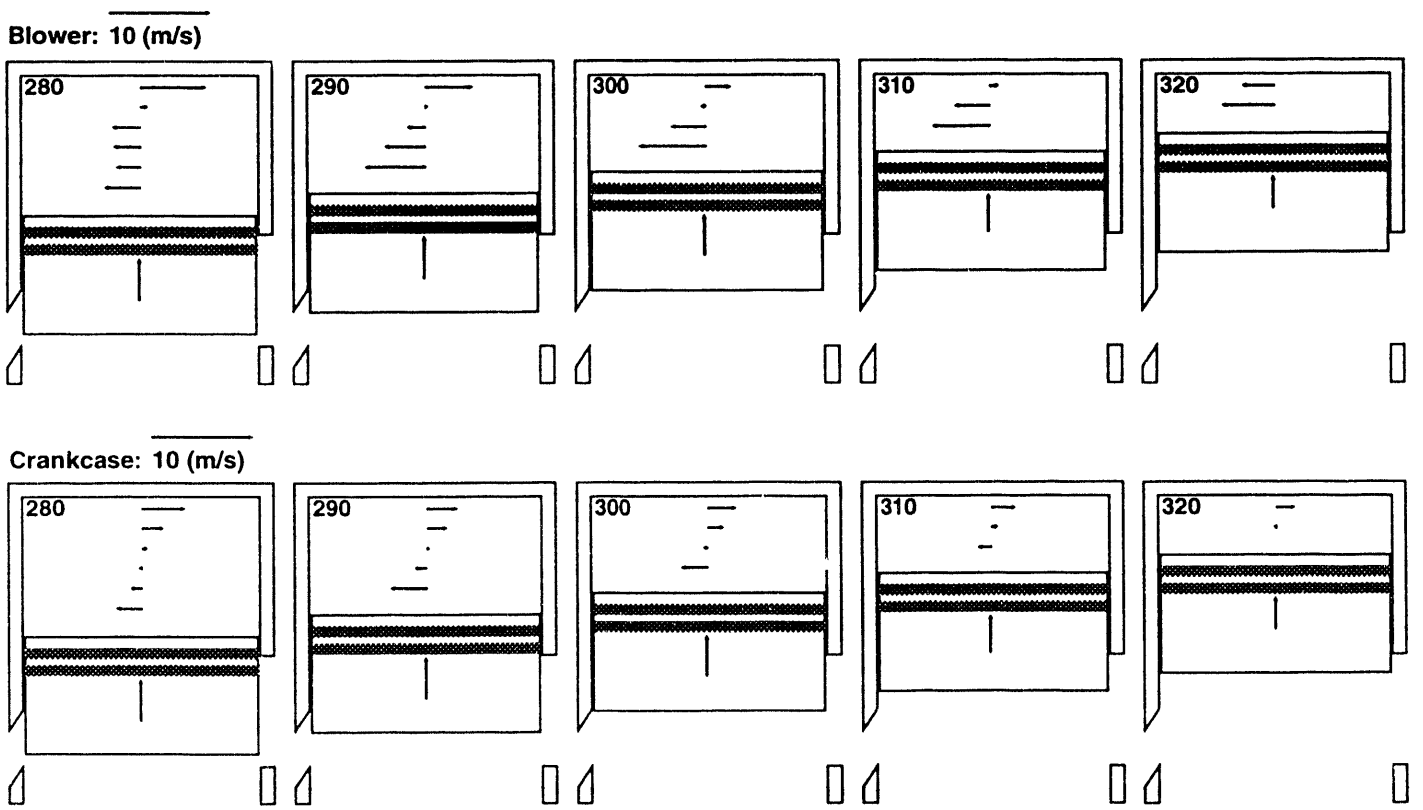

Fig. 15 Comparison of blower and crankcase scavenged velocity profiles during compression for DR=0.60. The crank-angle for each profile is given in the upper left corner of each figure.

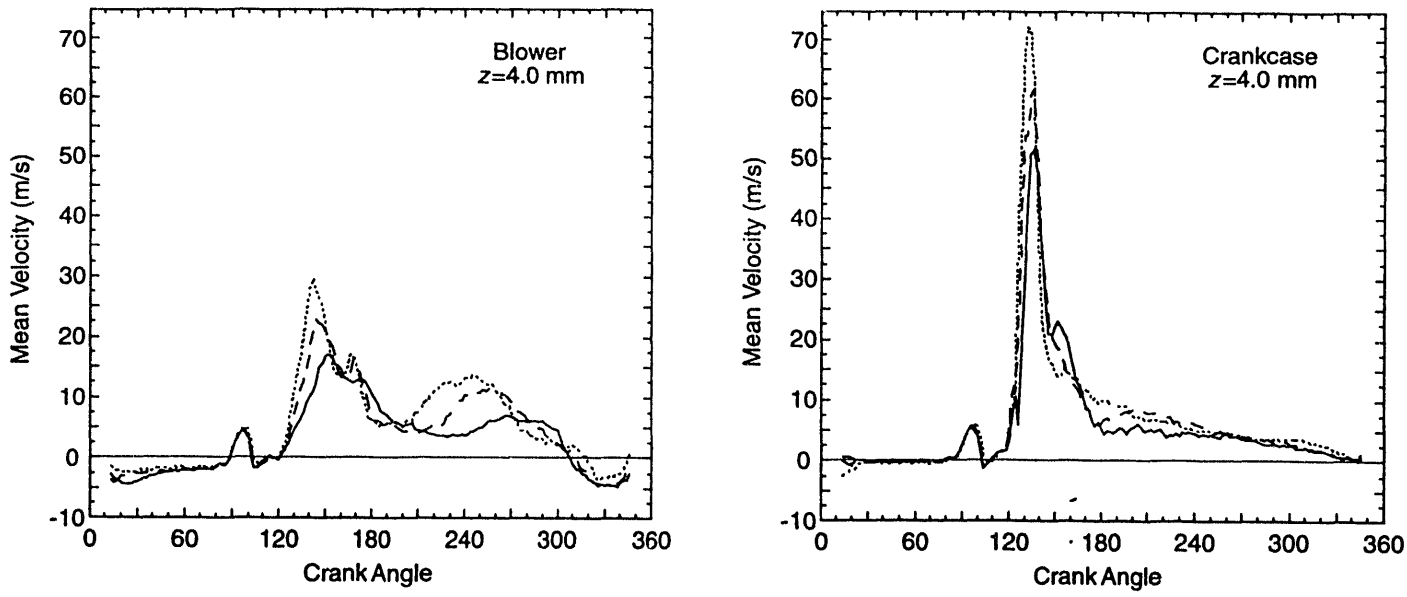

a) Mean velocity histories at z=4.0 mm.

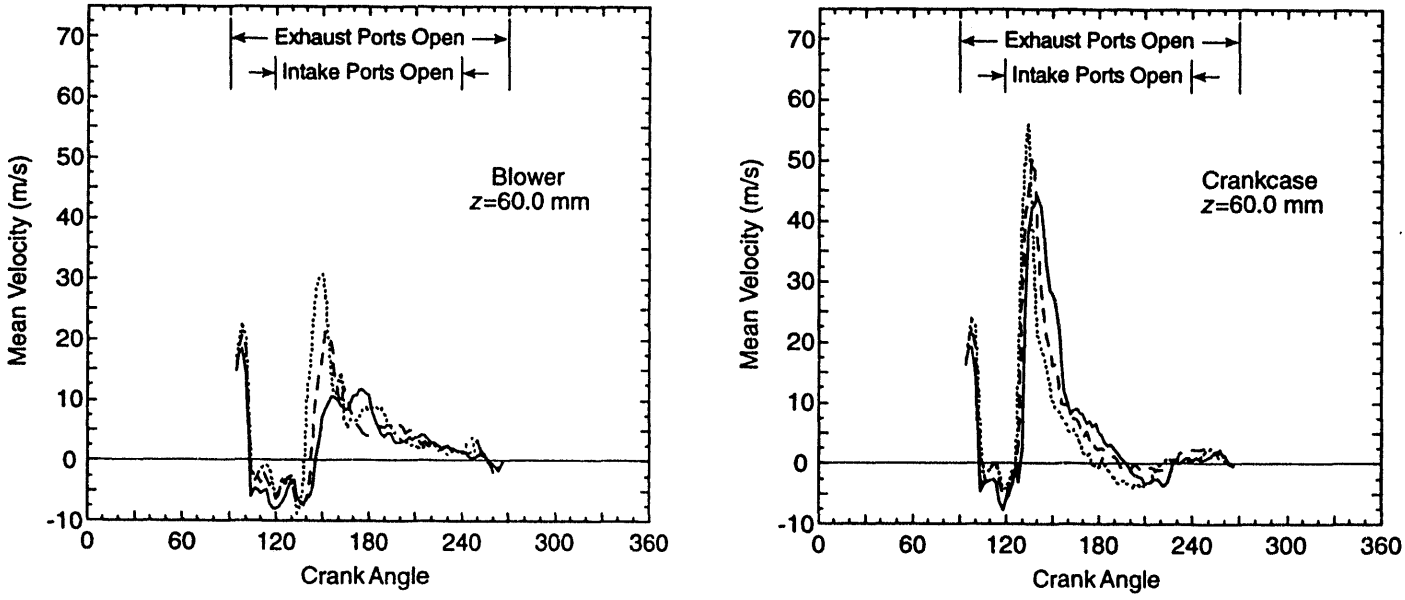

b) Mean velocity histories at z=60.0 mm.

Fig. 16 Comparison of blower and crankcase scavenged mean velocity histories for different delivery ratios. a.) z=4.0 mm from top of cylinder. b.) z=60.0 mm, slightly above top of exhaust port. —— DR=0.40; – – DR=0.60; ····· DR=0.80.

features of the BLS and CCS flows discussed above are preserved.

For z=4 mm there is no discernible difference in the velocities up to IPO, whereas at z=60 mm the blowdown velocities are slightly larger for higher delivery ratios, and the negative flow overshoot has the opposite trend. This behavior is consistent with a backflow from the exhaust manifold induced by cylinder volume expansion. As the delivery ratio increases, blowdown and exhaust manifold velocities increase, and the flow induced by piston motion is impeded by the inertia of the manifold gases. At IPO the expected behavior is seen, including a significantly stronger dependence on delivery ratio for BLS. Following the maximum velocity point, the deceleration of the flow appears to be insensitive to delivery ratio for CCS at z=4 mm, but at z=60 mm it is quite sensitive, with the lower delivery ratio having the highest velocities. This would seem to be indicative of greater penetration into the upper region of the

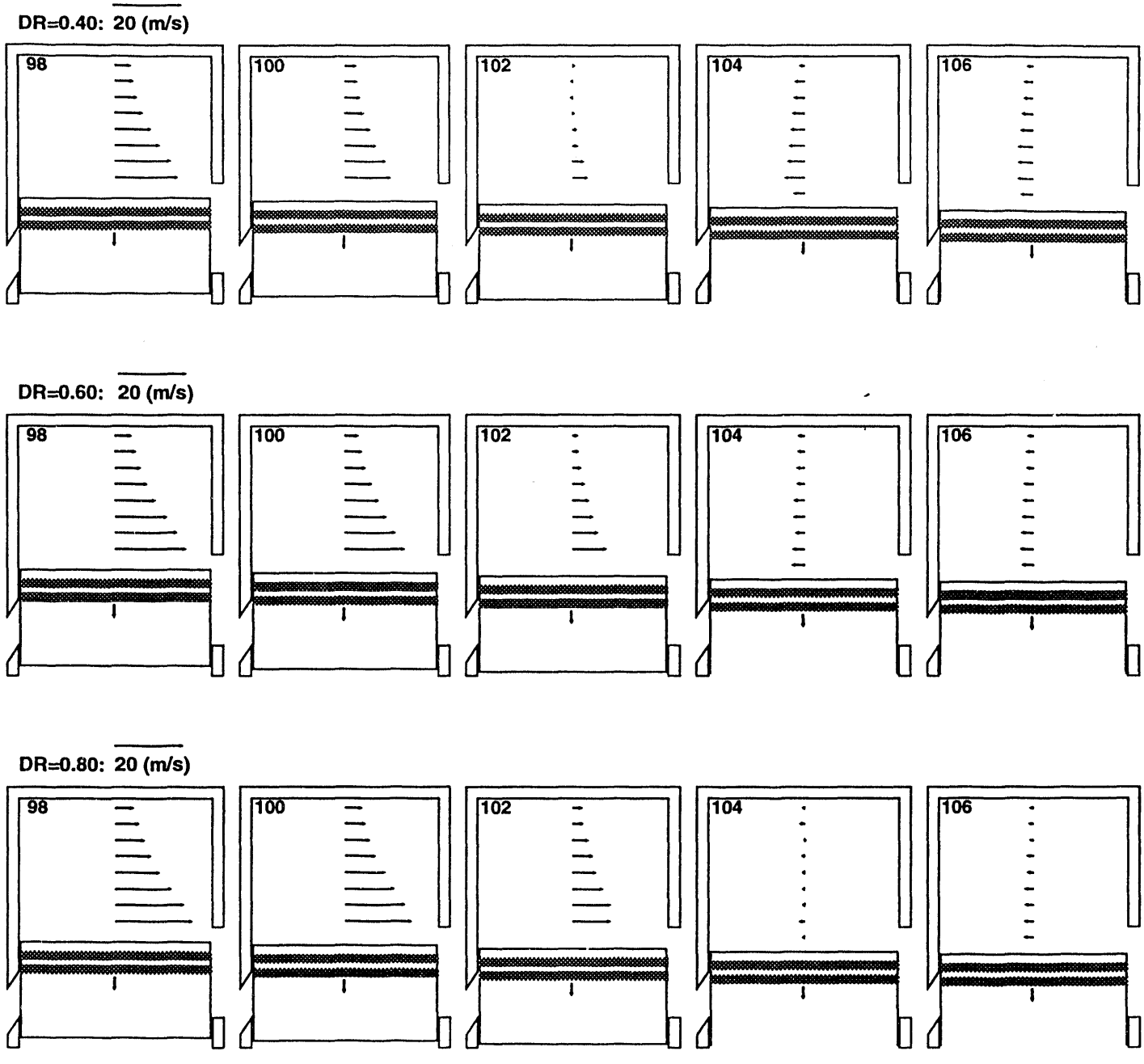

Fig. 17 Blower scavenged velocity profiles near the end of blowdown for different delivery ratios.

combustion chamber for higher delivery ratios. After EPC, there is little difference in the velocities at z=4 mm.

For BLS after BDC, the velocities at z=60 mm are fairly insensitive to delivery ratio, whereas at z=4 mm the very opposite exists. The late scavenging period velocity profiles presented earlier in Fig. 14 indicated that new jets of high velocity fluid are directed toward the top of the chamber as the intake ports close. The differences in the phasing and magnitude of the second maxima in velocity indicate that these new jets are both stronger and penetrate earlier to the top of the chamber as the delivery ratio increases.

Because there is reasonable similarity in the velocity measurements for the different delivery ratios, we have chosen to present velocity profile comparisons for only the more interesting portions of the cycle. Shown in Fig. 17 is the end of the blowdown period for BLS. The profiles are displayed with 2 CAD resolution to illustrate how rapid the flow-direction reversal is between 100 and 104 CAD. The velocity profiles are quite similar for the different delivery ratios; whereas the magnitude of the early positive flow is greater for higher DR, the later negative flow is greater for lower DR. The corresponding blowdown profiles for CCS are nearly identical.

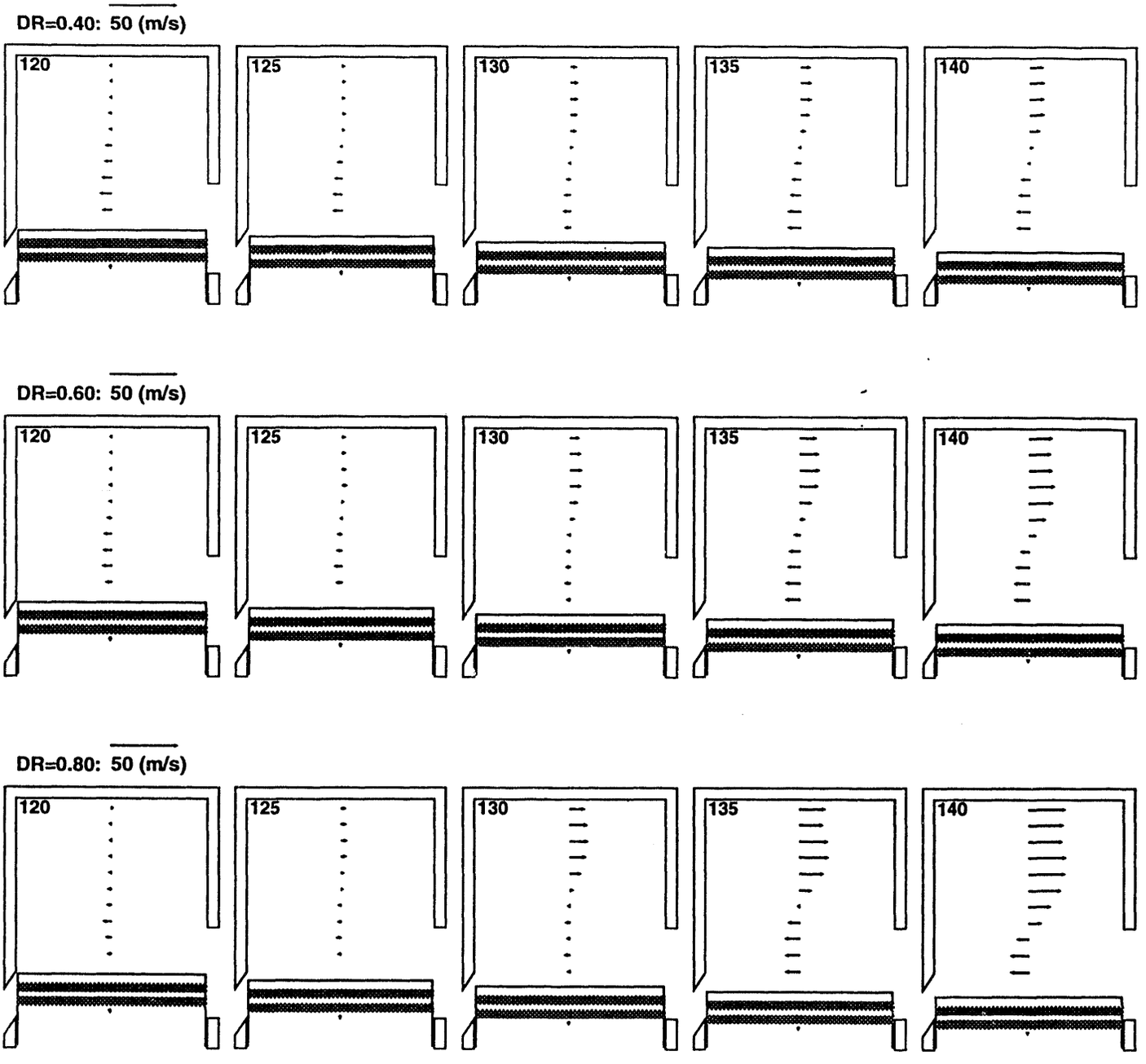

Fig. 18 Blower scavenged velocity profiles during early scavenging for different delivery ratios.

BLS velocity profiles for the early scavenging period are compared in Fig. 18. The profiles are quite similar for the different delivery ratios, with the exception that the center of the tumble vortex is closer to the piston for higher delivery ratios. A similar behavior is seen for CCS in Fig. 19, except that the tumbling motion is established earlier, and its center moves toward the piston earlier and more rapidly, such that a uniformly positive centerline profile appears earlier than for BLS. In essence, the greater the early rate of fresh charge delivery, be it by CCS or by greater delivery ratio, the earlier is the formation of a tumble vortex and the more rapid is the appearance of a uniformly positive velocity profile.

RMS VELOCITY STATISTICS

RMS velocity histories (i.e., ensemble-averaged mean fluctuating velocities) measured at z=4 mm are summarized in Fig. 20. Prior to IPO these data are not particularly interesting; there is some increase in the velocity fluctuations at EPO, but it is not of significance to the scavenging process. Soon after IPO, however, there is a very rapid increase in the rms velocity that corresponds to both turbulence in the flow and phase differences, or cyclic variability, in the arrival time of the large velocity gradients accompanying the incoming charge (refer to Fig. 16a). During this initial intake period

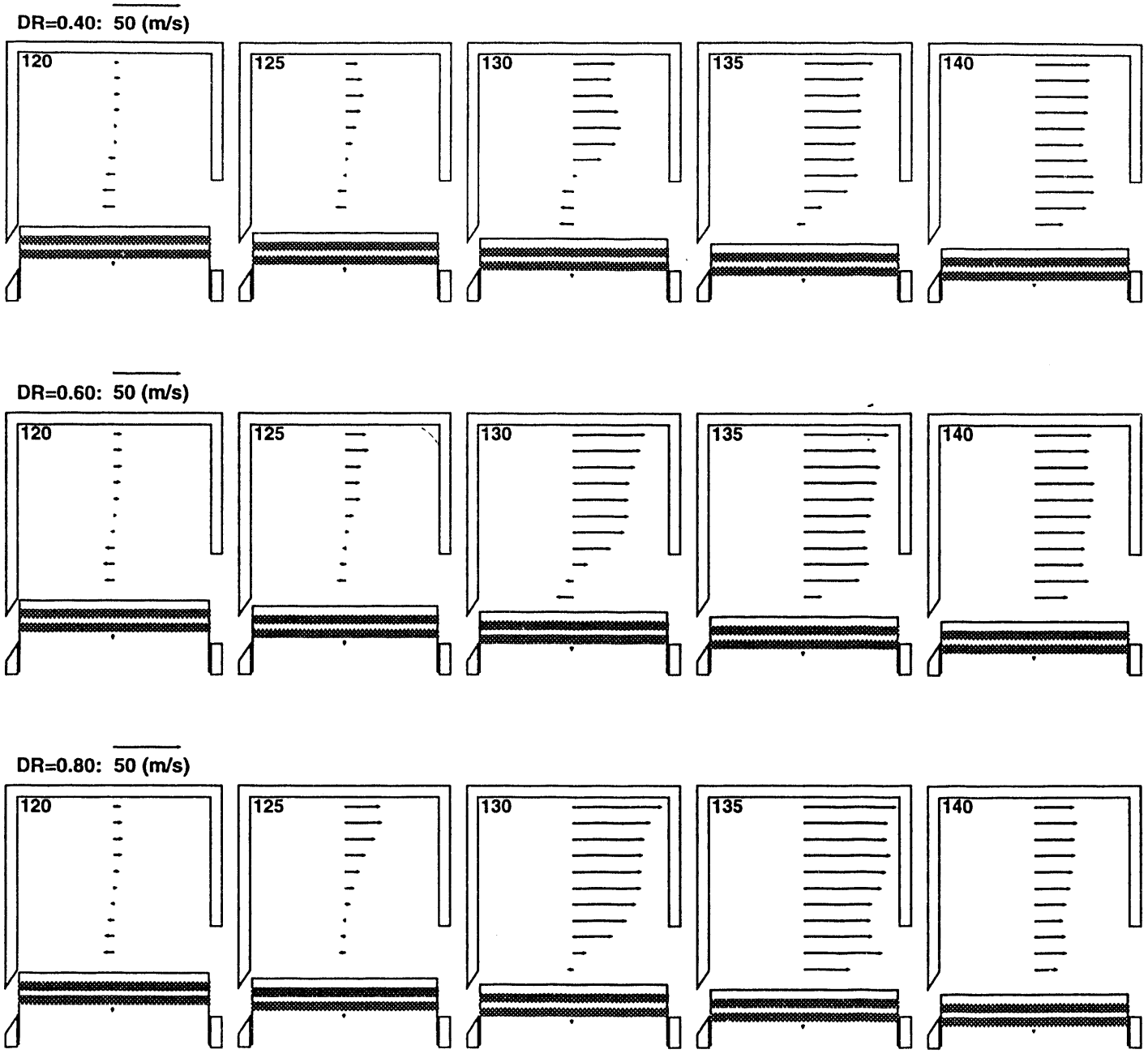

Fig. 19 Crankcase scavenged velocity profiles during early scavenging for different delivery ratios.

the peak rms velocity varies only slightly with delivery ratio for CCS; the variation is far greater for BLS. Referring to Fig. 16, the peak velocities for CCS do vary with delivery ratio at this location, suggesting to us that the expected behavior for the rms velocity should be similar. The observed lack of similarity may imply that as the delivery ratio increases the CCS flow is less susceptible to cycle-to-cycle variations in phasing and magnitude.

Following the large rms velocity peak corresponding to the main intake flow, both BLS and CCS exhibit a general increase in fluctuations around BDC, although this increase is more pronounced for CCS. Referring again to the mean velocity results in Fig. 16, for all but the case of CCS at DR=0.80 there is a distinct pattern of a decelerating velocity up to BDC, followed by a relative constant velocity period; this flat period comes slightly later for BLS at DR=0.40. These velocity patterns can be expected to lead to an increase in the rms velocity prior to BDC, but not after BDC. The velocity profile measurements shown earlier in Fig. 13, however, reveal a significant mean shear stress for CCS during this period in the upper regions of the cylinder.

Finally, during the latter stages of the compression process for CCS the velocity fluctuations are seen to increase slightly, with little dependence on the delivery ratio. In contrast, for BLS the fluctuations are quite varied

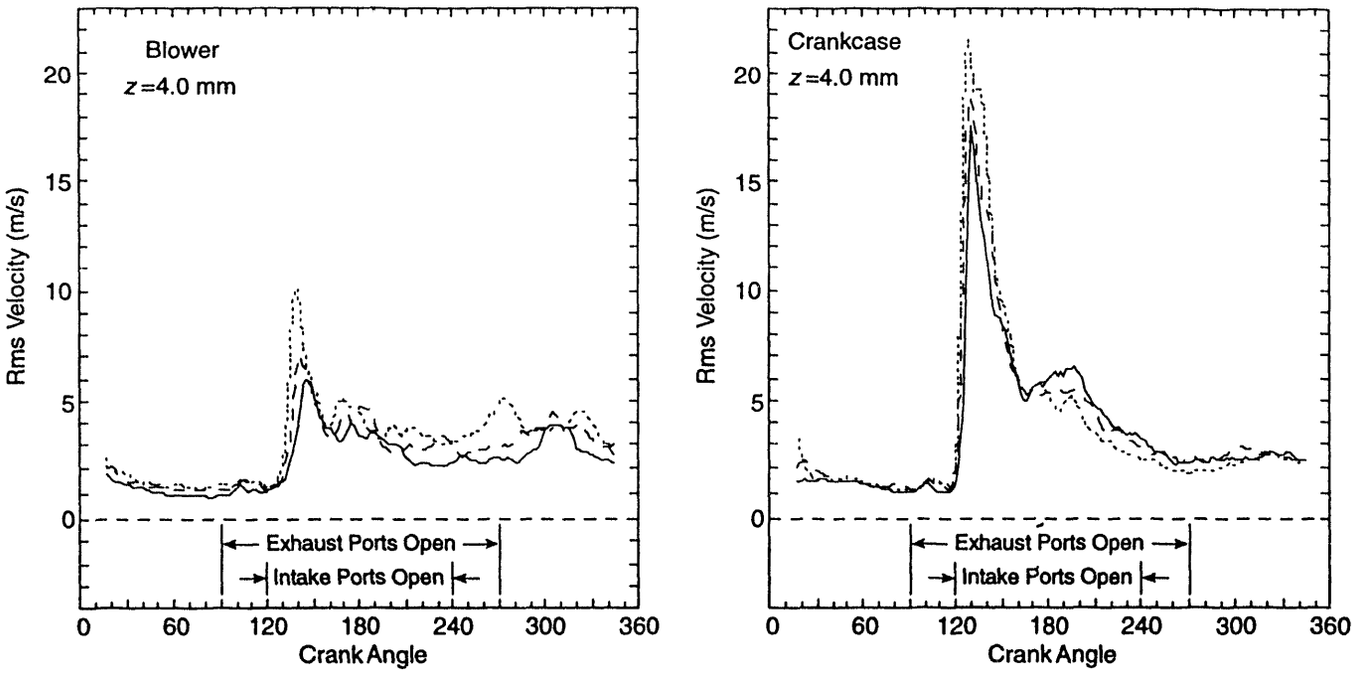

Fig. 20 Rms velocity fluctuations at z=4.0 mm. ——— DR=0.40; - - - - - DR=0.60; ---------- DR=0.80.

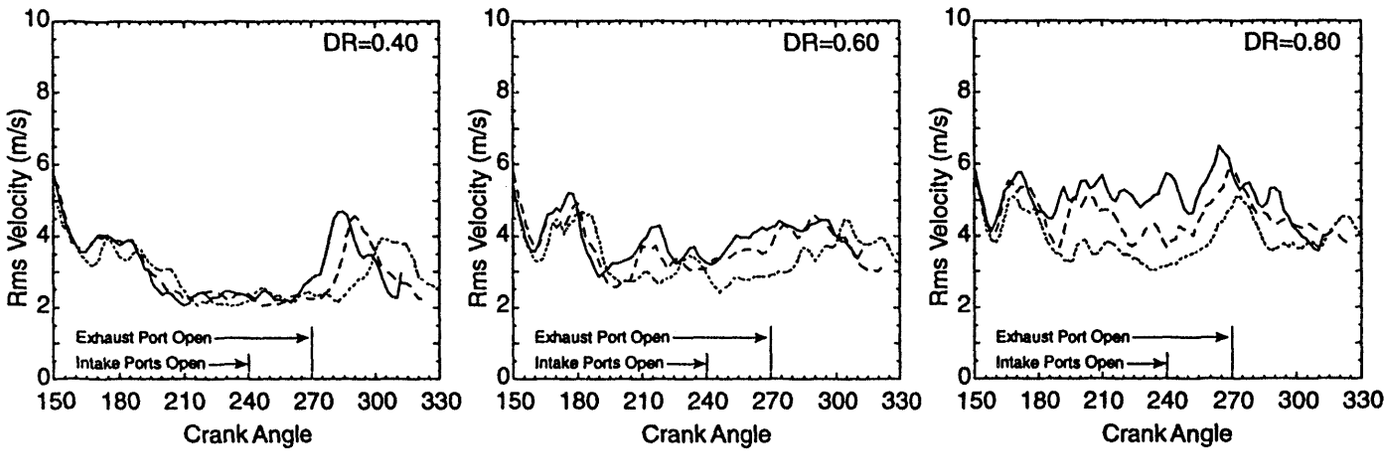

a) Blower scavenged RMS velocities.

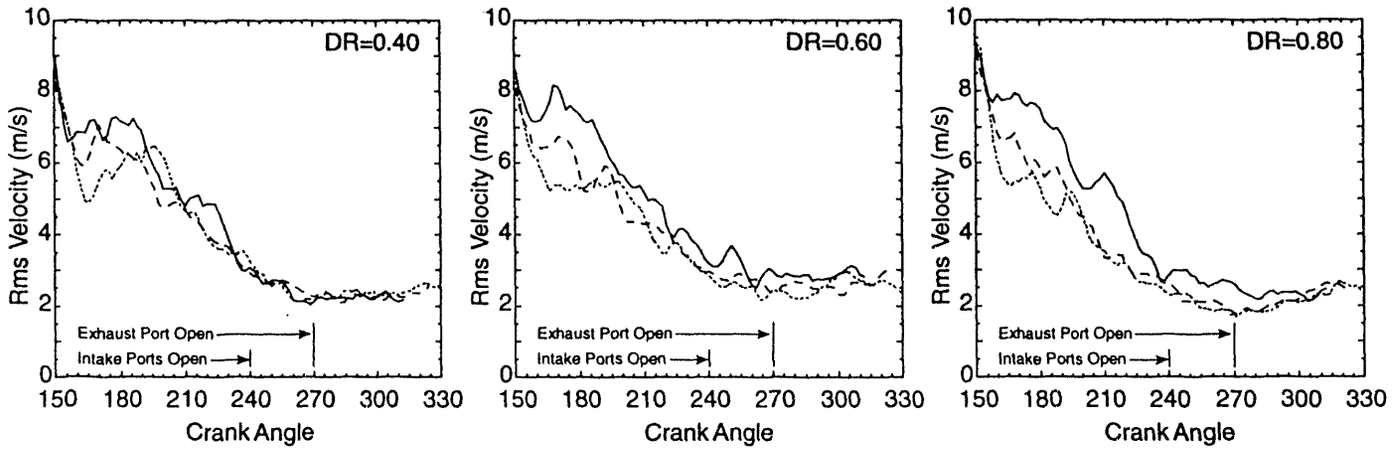

b) Crankcase scavenged RMS velocities.

Fig. 21 Expanded-scale RMS velocity histories for the three upper measurement locations. a.) Blower scavenged. b.) Crankcase scavenged. ---- z=4.0 mm; - - z=12.0 mm; —— z=20.0 mm.

in both amplitude and phasing for the different delivery ratios. These differences can be seen more clearly in Fig. 21, where the rms velocity fluctuations during the compression stroke are presented for the three upper measurement locations. In general, the flow field is far more homogeneous for CCS, and the fluctuating velocities are also considerably less than for BLS.

SUMMARY AND CONCLUSIONS

Although the data presented and discussed above show consistent and distinct features characterizing the BLS and CCS flow fields, it is stressed that velocity measurements were made for only one component of velocity along the cylinder axis. We believe that this sampling is sufficient to resolve many distinguishing features of the flow fields. Nevertheless, the scavenging flows likely contain additional large scale structures which we have been unable to resolve. It must be recognized, therefore, that the following summary does not constitute a complete and definitive description of the in-cylinder flow.

- Statistics of in-cylinder pressure indicate that combustion is more rapid, with less cyclic variation, under BLS conditions. This may be due to: 1) better scavenging performance, 2) stratification of fresh mixture and residuals, such that more fresh mixture is present near the spark, or 3) higher levels of turbulence during the combustion process.

- Differences in the mean velocity fields between blower and crankcase scavenging persist throughout the cycle until exhaust port opening.

- The velocity fields during cylinder blowdown are quite similar for both scavenging methods, and blowdown is complete well before intake port opening. A backflow into the cylinder after blowdown persists until intake port opening. This backflow is probably due primarily to continued cylinder volume expansion with piston motion, with secondary influence from exhaust manifold dynamics.

- During the early scavenging period, both the BLS and CCS flows are initially characterized by a dominant, large tumble vortex structure. The CCS flow subsequently evolves to a structure characterized by radial flow toward the exhaust port along the entire cylinder centerline. For both cases, the fresh charge appears to penetrate to the top of the combustion chamber. Both may be suitable for efficient scavenging of 'bowl-in-head' combustion chamber designs. This penetration appears to grow stronger with increasing delivery ratio.

- During the mid-scavenging period, the BLS flow evolves to one characterized by a uniformly positive radial velocity profile. The latter part of this evolution takes place in an abrupt transition. The CCS flow reverts to a rotating, tumble vortex pattern.

- Late in the scavenging process, the continued delivery of fresh charge under BLS conditions promotes the formation of more energetic, large-scale tumble motions as compared to the CCS flow.

- During compression, the energetic large-scale structures set up late in the scavenging process by the BLS flow produce higher shear in the axial direction. This large shear may result in enhanced production of turbulence.

- The major features of both the BLS and CCS flow fields are quite insensitive to changes in delivery ratio. Although the phasing and magnitude of these features vary, the general nature of the flow does not.

- RMS velocity fluctuations near the top of the combustion chamber confirm the expected enhanced production of turbulence under BLS conditions. Rms velocities are consistently higher during compression for the BLS flows, and the data indicate significant spatial variations. The lower rms velocity fluctuations characterizing the CCS flows are, in contrast, much more spatially homogeneous.

ACKNOWLEDGMENTS

The authors particularly wish to acknowledge E.G. Groff, T.D. Fansler, and W.R. Matthes of the General Motors NAO R&D Center for the design of the porting and transfer passages employed in this work, for the model results presented in Fig. 3, and for many helpful and illuminating discussions. Duane Sunnarborg has provided assistance with all mechanical aspects of this work, provided Figs. 1 and 2, and was responsible for the mechanical design of the fiber optic LDV probe. The probe optical design was heavily influenced by S.C. Bopp. We further wish to thank G.L. Hubbard for portions of the data acquisition software. This work was performed at the Combustion Research Facility of the Sandia National Laboratories, and was funded by the U.S. Department of Energy, Advanced Industrial Concepts Division.

REFERENCES

1. Wyczalek, F.A., "Two-Stroke Engine Technology in the 1990's," SAE Paper No. 910663, 1991.

2. Groff, E.G., Fansler, T.D. and Matthes, W.R., General Motors NAO R&D Center, Warren, MI, private communication, 1993.

3. Green, R.M. and Cousyn, B.J., "An Optical Research Engine for the Study of Two-Stroke Cycle In-Cylinder Phenomena," COMODIA 90, International Symposium on Diagnostics and Modeling of Combustion in Internal Combustion Engines, Kyoto, Japan, 1990.

4. Bopp, S.C., Cousyn, B.J., Green, R.M. and Witze, P.O., "Experimental Study of the Scavenging and Combustion Processes in a Two-Stroke Cycle Research Engine," *Trans. SAE* **101**, Sec. 3, p. 245, 1992.

5. Groff, E.G., General Motors NAO R&D Center, Warren, MI, private communication, 1993.

6. Morel, T., Flemming, M.F. and LaPointe, L.A., "Characterization of Manifold Dynamics in the Chrysler 2.21 S.I. Engine by Measurements and Simulation", SAE Paper No. 900679, 1990.

7. Ikeda, Y., Ohhira, T., Takahashi, T. and Nakajima, T., "Misfiring Effects on Scavenging Flow at Scavenging Port and Exhaust Pipe in a Small Two-Stroke-Engine," SAE Paper No. 930498, 1993.

8. Obokata, T., Hanada, N. and Kurabayashi, T., "Laser Doppler Anemometer Measurement of Gas Flow in the Wedge-Type Combustion Chamber of a Two-Cycle Spark Ignition Engine," Combustion in Engines - Technology and Applications, Institution of Mechanical Engineers, Mechanical Engineering Publications Ltd., p.213, 1988.

9. Fansler, T.D. and French, D.T., "The Scavenging Flow Field in a Crankcase Compression Two-Stroke Engine - A Three Dimensional Laser Velocimetry Survey," *Trans. SAE* **101**, Sec. 3, p. 581, 1992.

10. Okuyama, L., Kousaka, Y., Tohge, N., Yamamoto, S., Wu, J.J., Flagan, R.C. and Seinfeld, J.H., "Production of Ultrafine Metal Oxide Aerosol Particles by Thermal Decomposition of Metal Alkoxide Vapors," *AIChE J.* **32**, No. 12, p. 2010,1986.

11. Witze, P.O. and Baritaud, T.A., "Particle Seeding for Mie Scattering Measurements in Combusting Flows," Proceedings of the Third International Symposium on Applications of Laser Anemometry to Fluid Mechanics, Lisbon, July 1986.

APPENDIX

Figures A1 and A2 illustrate the relationship of the in-cylinder velocity, the intake manifold pressure, and the exhaust manifold pressure during the period in which the ports are open. The velocity/crank-angle history shown was obtained at z=60 mm, a location low enough in the cylinder to expect good coupling with the manifold pressure fluctuations, yet high enough to obtain the velocity record throughout the time the ports are open. Intake and exhaust manifold pressures were monitored with 0.165 MPa and 0.662 MPa differential pressure transducers (Validyne Model P24), respectively. The signal from the exhaust transducer was subsequently amplified by 10 prior to digitization.

During the period prior to IPO at 120 CAD, the coupling between the in-cylinder velocity and the exhaust manifold pressure is quite evident. The BLS velocity history reflects the variations in the exhaust manifold pressure particularly well. Note that the negative velocities characteristic of the backflow into the cylinder appear to be perturbed by the exhaust pressure fluctuations, but not driven by them. From IPO to about 130 CAD the velocity behavior is ambiguous, but beyond 130 CAD, the flow is dominated by the intake jets. Some velocity perturbations associated with the exhaust pressure are still apparent in the BLS case, however. Beyond 130 CAD the flows are clearly affected only slightly by the variations in the intake and the exhaust manifold pressures. These features are quite interesting, in that they appear to imply that the effects of the manifold pressure wave dynamics only slightly affect the central portion of the in-cylinder flow, and that the general scavenging flow patterns are relatively independent of the specific manifold geometries employed.

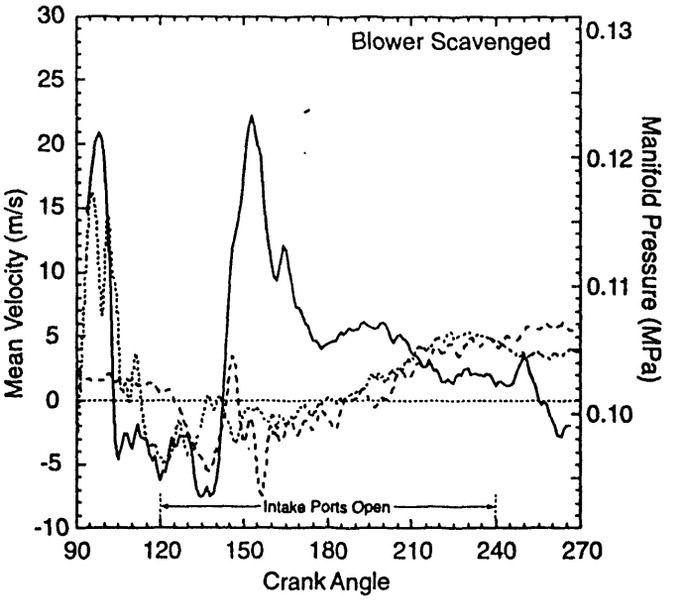

Fig. A1 Blower scavenged velocity and manifold pressure histories. —— Mean velocity, z=60.0 mm; ---- Intake manifold pressure; ····· Exhaust manifold pressure.

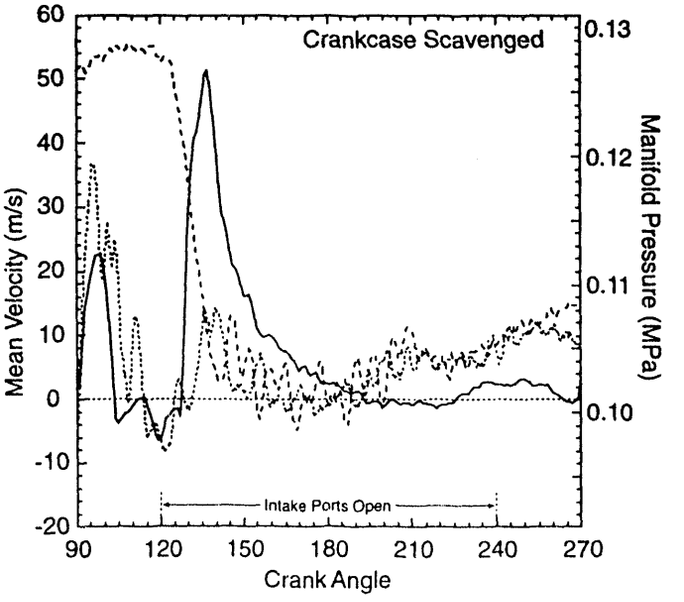

Fig.A2 Crankcase scavenged velocity and manifold pressure histories. —— Mean velocity, z=60.0 mm; ---- Intake manifold pressure; ····· Exhaust manifold pressure.

END

DATE
FILMED
3/9/94